Geomorphic expressions of active rifting reflect the role of structural inheritance: A new model for the evolution of the Shanxi Rift, North China

Malte Froemchen[1], Ken J. W. McCaffrey[1], Mark B. Allen[1], Jeroen van Hunen[1], Thomas B. Phillips[1], Yueren Xu[2]
[1]Department of Earth Sciences, Durham University, Science Labs, Durham, DH13LE, UK
[2]Key Laboratory of Earthquake Prediction, Institute of Earthquake Forecasting, China Earthquake Administration, Beijing, China

Correspondence to: Malte Froemchen (malte.froemchen@durham.ac.uk)

Abstract. Many rifts are influenced by pre-existing structures and heterogeneities during their evolution, a process known as structural inheritance. During rift evolution, these heterogeneities may aid rift nucleation, growth, and segmentation of faults, encourage linkage of various segments, or even inhibit the formation of faults. Understanding how structural inheritance influences early rift evolution could be vital for evaluating seismic risk in tectonically active areas. The Shanxi Rift in the north of China is an active rift system believed to have formed along the trend of the Proterozoic Trans North China Orogen, however, the influence of these pre-existing structures on the present-day rift architecture is poorly known. Here we use tectonic geomorphological techniques, e.g., hypsometric integral (HI), channel steepness (k_{sn}) and local relief to study the evolution of the Shanxi Rift and identify areas of higher tectonic activity. We found that HI was less sensitive to lithology and more valuable in evaluating the tectonic signal and found that activity is concentrated in two rift interaction zones (RIZ) formed between the Xinding, Taiyuan, and Linfen basins. We then evaluated the relationship between the active faults and mapped pre-existing structures and found that many faults formed parallel to inherited structures but faults in the RIZs often crosscut these structures. Based on these observations we propose a new model for the evolution of the Shanxi Rift where inherited structures play an important part in the initial segmentation of the rift which in turn controls the development of the RIZ structures.

Deleted: evaluate

1 Introduction

Many continental rifts exploit ancient orogenic belts to accommodate extensional strain. Examples include East African Rift (Rosendahl, 1987; Morley, 1988; Ring, 1994), Baikal Rift (Petit et al., 1996), and the Rhine Graben (Schuhmacher, 2002). Research has focused on understanding the relationship between old pre-rift structures and how they control the development of younger structures. Pre-existing orogenic belts influence the accommodation of subsequent episodes of extensional strain, due to the presence of discrete and mechanically weak structures, such as shear zones and associated metamorphic fabrics (McCaffrey, 1997; Phillips et al., 2016, Fazlikhani et al., 2017; Kolawole et al., 2018; Peace et al., 2018; Heilman et al., 2019),

pre-existing fault networks (Holdsworth et al., 2001) or lithological contacts (Wedmore et al., 2020; Phillips and McCaffrey, 2019). These mechanical strength contrasts are particularly significant where orogenic belts are adjacent to cratons (Dunbar and Sawyer, 1988; Ziegler and Cloethingh, 2004; Corti et al. 2013) as is the case for the Baikal Rift (Petit et al. 1996), the East African Rift (Versfelt and Rosendahl, 1989) and the Circum-Ordos rifts in North China (Xu and Ma, 1992; Su et al., 2021), because cratonic lithosphere is more resistant to deformation than younger orogenic belts.

Studies of the interaction between rift-related normal faults and inherited structures in offshore basins and margins use high resolution 2D and 3D seismic reflection data to analyse the influence of inheritance on spatio-temporal patterns of rift evolution (Morley et al., 2004; Phillips et al., 2016; Peace et al., 2018, Mulaya et al., 2022). Detailed field studies, on the other hand, can resolve the kinematic response of faults and infer strainfield directions and interactions (e.g., East Africa, Hodge et al., 2018b; Wedmore et al., 2020; Heilman et al., 2019; Kolawole et al., 2018). Inherited structures and heterogeneities can influence the location, morphology, segmentation, and orientation of an entire rift zone (Wilson et al., 1966; Tommasi and Vauchez, 2001; Şengör et al., 2019; Heron et al., 2019; Schiffer et al., 2020; Kolawole et al. 2022). They can also influence the geometry and kinematics of individual faults (Wedmore et al., 2020; Samsu et al., 2020; Wilson et al., 2010). Inherited structures can influence the development of rifts and their associated basins by controlling linkage of fault segments (Brune et al., 2017; Heilman et al., 2019). Pre-existing structures have also been shown to act as barriers to rift faults if they form structures or regions of strengthened crust that is harder to deform than surrounding areas (Krabbendam and Barr, 2000; Phillips and McCaffrey, 2019).

Many rifts that show a strong influence of inheritance are very segmented and exhibit numerous faults and basins that vary in orientation and morphology (Morley et al., 2004; Reeve et al., 2015; Heron et al., 2019; Osagiede et al., 2020). Between individual basins of a rift zone, a complex deformation zone known as Rift Interaction Zone (RIZ) may develop (Nelson et al., 1992; Koehn et al., 2008; Aanyu and Koehn, 2011; Sachau et al., 2016; Kolawole et al., 2021a). The morphology of these zones is principally controlled by the separation distance between fault segments, the polarity of the respective faults and the amount of overlap between them (Morley et al., 1990; Faulds and Varga, 1998; Zwaan and Schreurs, 2017, Zwaan et al., 2016). RIZs are classified on their geometrical organisation (rift segment faults are underlapping or overlapping, parallel, oblique, or orthogonal). Commonly, these zones are topographically distinct from the rest of the rift. RIZs may form topographic highs in their early evolution, forming as a drainage divide between depocenters (Ebinger et al., 1987; Lambiase and Bosworth, 1995; Gawthrope & Hurst, 1993) and therefore acting as a source of sediment (Gawthrope and Hurst, 1993; Scholz, 1995). As RIZs evolve, they can become breached and eventually link up the rift basins (Kolawole et al., 2021a). RIZs can also be classified on their evolution stage (Kolawole et al., 2021a), i.e. whether the RIZ is unbreached, partially breached, recently breached, or breached. This is assessed based on two observations: 1) Presence of a breaching fault that extends from one rift segment to the other segment, and 2) Presence of an established physical linkage of depositional environments of both rift segments (i.e., drainage connection between both segments). Recently breached and breached RIZs have an established breaching fault and connect the drainage of two different rift segments, but breached RIZs shows less topography due to increased subsidence during the longer time period since the RIZ was breached. Unbreached RIZs show no apparent structural connection and no

Deleted: spatiotemporal

Deleted: Inherited

Deleted: 2021

Moved (insertion) [1]

Moved (insertion) [2]

drainage connection, while partially breached RIZs may have a breaching fault partially connecting the rift basins but the drainage integration has not occurred yet. RIZs may also show a perturbated local strain field due to the influence of the adjacent, bounding rift faults (Crider and Pollard, 1998; Kattenhorn et al., 2000; Maerten, 2000; Kolawole et al., 2024). Development of these zones may be aided by basement fabrics that strike oblique to the main extension direction (Fossen and Rotevatn, 2016); however, basement fabrics may also influence linkage across these zones (Morley et al., 2004; Heilman et al., 2019; Kolawole et al., 2021a). RIZs are important structural domains along rift systems, and inheritance may be key to understanding their geometry and evolution.

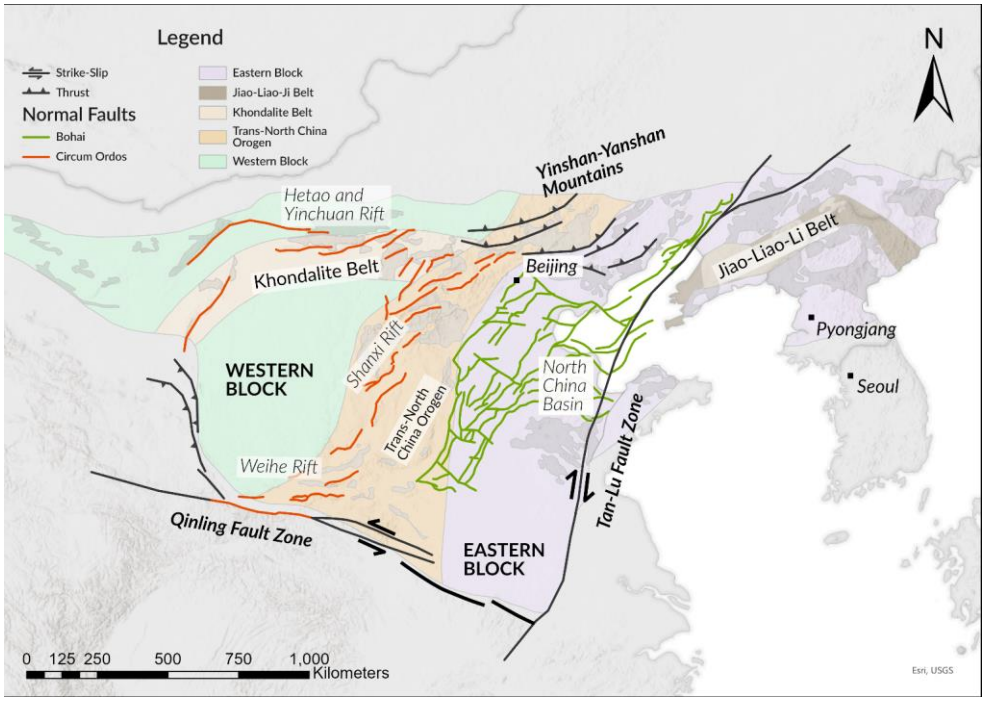

Figure 1: Overview map of the North China Craton (NCC) with boundaries of the different blocks and orogenic belts that make up the NCC shaded in colour. Boundaries after Zhao et al. 2005. Also indicated are the two major rift systems that formed superimposed on the NCC: The Paleogene North China Basin (in green, modified from Qi and Yang, 2010) and the Neogene circum-Ordos Rifts (in red, modified from Zhang et al., 2003; Deng et al., 2007). Bold black lines indicate the major strike-slip fault zones that effect present-day deformation.

Deleted: 2021).

Deleted: 2021

Deleted:

The Shanxi Rift is part of a Cenozoic rift system which is known as the Circum-Ordos rifts, which surrounds the Western Block of the North China Craton (NCC) (Fig.1). Due to the strong lithosphere of the cratonic western block of the NCC, deformation was localised in two rift system along it: The Weihe-Shanxi Rift system in the southeast and the Yinchuan-Hetao rift system in the northwest (Zhang et al., 2003). Timing of the initiation of these rifts is debated with some authors arguing for Oligocene-Eocene initiation of the Weihe, Hetao and Yinchuan rifts, with the Shanxi Rift being younger (Zhang et al., 2003; Shi et al., 2020), while other authors argue for a late Miocene initiation for all rifts (Yin, 2000). The Shanxi Rift in North China contains faults with a variety of trends which formed in the Late Miocene to present day (Su et al., 2023) (Fig.1). The origin of these trends is unclear but the currently accepted model postulates multiple changes in stress axes orientation during transtensional evolution of the Shanxi Rift since the late Miocene, with strain being partitioned into dip-slip and strike-slip fault systems during transtension (Shi et al., 2015a). There has been little focus on the influence of structural inheritance on the wider evolution of North China, with a few exceptions that show active normal faults often following the trends of inherited structures (Su et al., 2021) and possibly detaching into low angle shear zones at depth (Pavlides et al., 1999). Major faults in the Shanxi Rift commonly expose basement massifs of the Trans North China Orogen (TNCO) in their footwalls. The TNCO formed during the collision of the Eastern and Western Block of the NCC in the Paleoproterozoic. While these basement massifs have been intensively studied to unravel the exact timing and kinematics of the Proterozoic collision (Kusky and Li, 2003; Zhao et al., 2005; Trap et al., 2007, Trap et al., 2008; Faure et al., 2007; Trap et al., 2009a; Trap et al., 2009b; Zhai et al., 2010; Zhai and Santosh, 2011), their impact on the late Cenozoic rifting in the Shanxi Rift has not been considered in detail.

There is limited seismic reflection data available for the Shanxi Rift (Xu et al., 1993; Ai et al., 2019). However, the degree of tectonic activity and subaerial exposure makes it possible to use geomorphology to study the structural evolution. In active rifts geomorphology and surface expression of faults have been commonly used to study the tectonic evolution of a rift and successfully employed in regions such as the Basin and Range (Jackson and Leeder, 1994; Densmore et al., 2003; Densmore et al., 2004), the Apennines (Whittaker et al., 2008; Geurts et al., 2020; Fisher et al., 2022), the Gulf of Corinth (Leeder and Jackson, 1993; Goldsworthy and Jackson, 2000; Gallen et al., 2021) or the East African Rift (Erbello et al., 2022; Dulanya et al., 2022). These geomorphic approaches are varied and include studying the drainage evolution, the topographic response to faulting or using rivers to track the transient uplift rate. Landscapes are primarily formed by two competing forces: tectonics and erosion (Whittaker, 2012). Geomorphic indices have been used to quantify landscape response to tectonics (Bull and McFadden, 1980; Cox et al., 1994; Hamdouni et al., 2008; Gao et al., 2016; Markrai et al., 2022). This study uses three indices, hypsometric integral, channel steepness and local relief, to evaluate the landscape response to faulting in the Shanxi Rift.

By using geomorphic analysis to evaluate the tectonic evolution of the Shanxi Rift, highlighting areas of increased tectonic activity, and comparing these with the distribution of inherited structures, we provide new insights on the influence of inheritance on the evolution of the Shanxi Rift. Specifically, our results question the need for rapid changes in the Neogene strain field orientation to explain the varying fault orientations and fault evolution in the Shanxi Rift. Instead, we show a novel, simpler model whereby inheritance under a constant strain field creates a segmented rift system and creates RIZs where strain

Deleted: surround

Deleted: .

Deleted: .

Deleted: .

Deleted:)

Deleted: .

Deleted: follow

Deleted: .

Deleted: detach

Deleted: .

Deleted: the role of these basement massifs

Deleted: is a

Deleted: , that has been

and earthquake activity are focused. More generally, our work shows how geomorphic indicators can be used to identify the most active (and potentially hazardous) faults in an active extensional system.

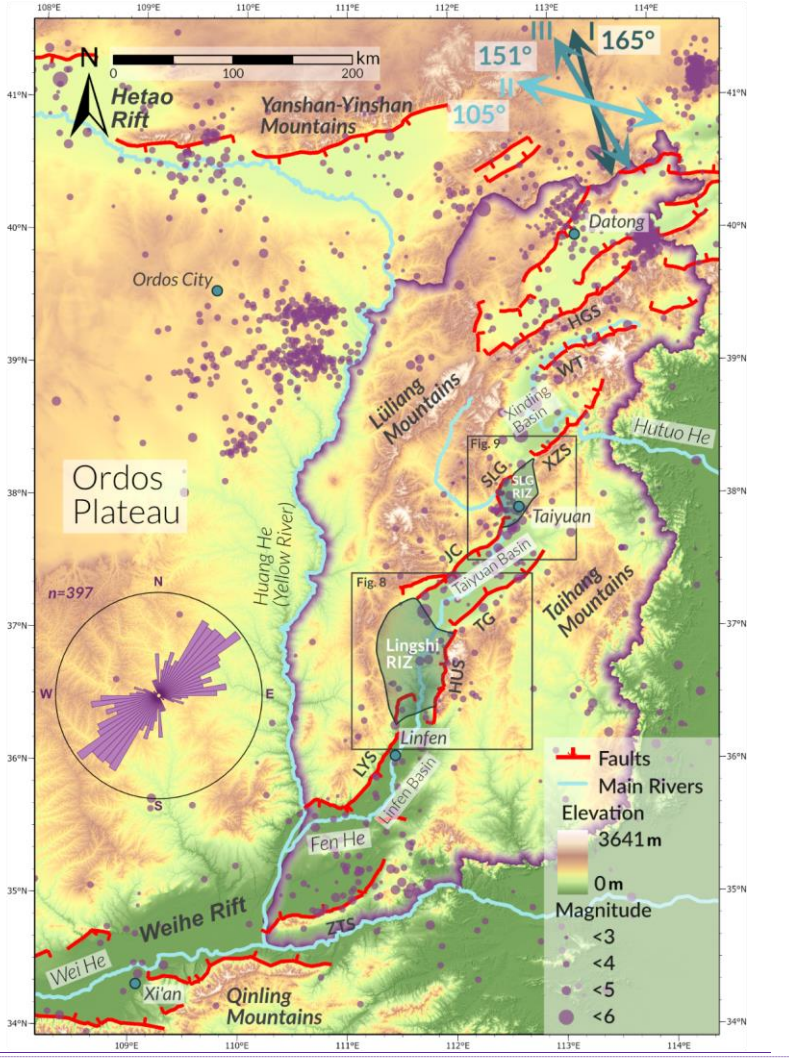

Deleted:

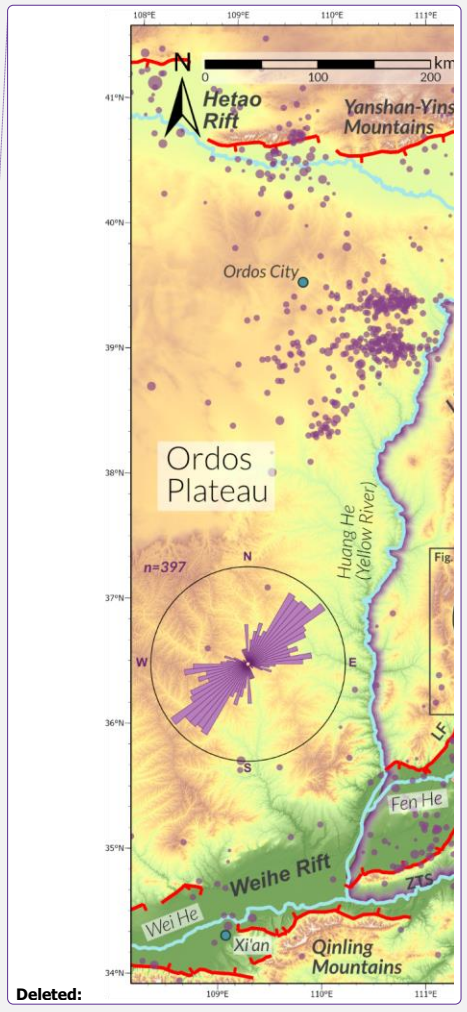

Figure 2: Detailed map of the circum-Ordos Rifts and the main rivers. Extension directions shown are from: I - Zhang et al. (1998) II - Shen et al. (2000) III - Middleton et al. (2017). Rose plot shows the mean orientation of major rift faults in the Shanxi Rift (defined here as the regions that lie within the purple bounding line). Faults were split into individual segments according to their orientation. Purple dots represent earthquakes from the ISC catalogue (Storchak et al., 2013; 2015; Di Giacomo et al., 2018) and are weighted by magnitude. (Abbreviations: HGS-Hengshan; WT-Wutai; XZS-Xizhoushan; SLG-Shilingguan; JC-Jiaocheng; TG-Taigu; HUS-Huoshan; LYS-Luosyunshan; ZTS-Zhongtiaoshan)

Deleted: LF-Linfen

2 Geological Setting

The Shanxi Rift system in North China is an active continental rift system that is superimposed on the 1.8 Ga TNCO (Fig. 1) when collision of the Eastern and Western Blocks formed the NCC. Exact timing and kinematics of this collision remain uncertain (Zhao et al., 2005; Kusky et al., 2007; Zhai and Santosh, 2011). Since the Proterozoic, the NCC has been a stable cratonic block with a lithospheric thickness of 200 km, evidenced by Palaeozoic kimberlites (Menzies et al. 1993; Griffin et al., 1998; Menzies et al., 2007). The Paleoproterozoic and Archean basement rocks are unconformably overlain by the greenschist facies metasedimentary rocks (Faure et al., 2007) of the Paleoproterozoic Hutuo Group, which was deposited in a foreland basin during the TNCO Orogeny (Li et al., 2010). The lower Palaeozoic cover consists of Cambrian continental siliclastic successions, followed by shallow marine carbonates and Ordovician platform carbonates. Carboniferous and Permian rocks were deposited in changing shallow marine to fluvio-deltaic conditions and contain coal measures. These are topped by Mesozoic continental clastics, grading into cross-bedded aeolian sequences in the Jurassic (SBGMR, 1989). This evolution led to a clear division of lithologies in the Shanxi Rift, the Paleoproterozoic rocks, which include all the rocks that made up the TNCO, including Archean Tonalite-trondhjemite-granodiorite complexes, high-grade metamorphic rocks such as greenstone belts and orthogneisses as well as post-orogenic granites. These rocks are referred to as Paleoproterozoic crystalline rocks in this study (dark brown in Fig.3) and are very resistant to erosion. The second group comprises the cover sequence of these rocks and is principally composed of low-grade metamorphic rocks such as clastic metasediments and carbonates of Mesozoic and Palaeozoic age, which are referred to as low-grade metasediments in this study (blues and greens in Fig.3).

Deleted: .

Deleted: orogeny

Deleted: .

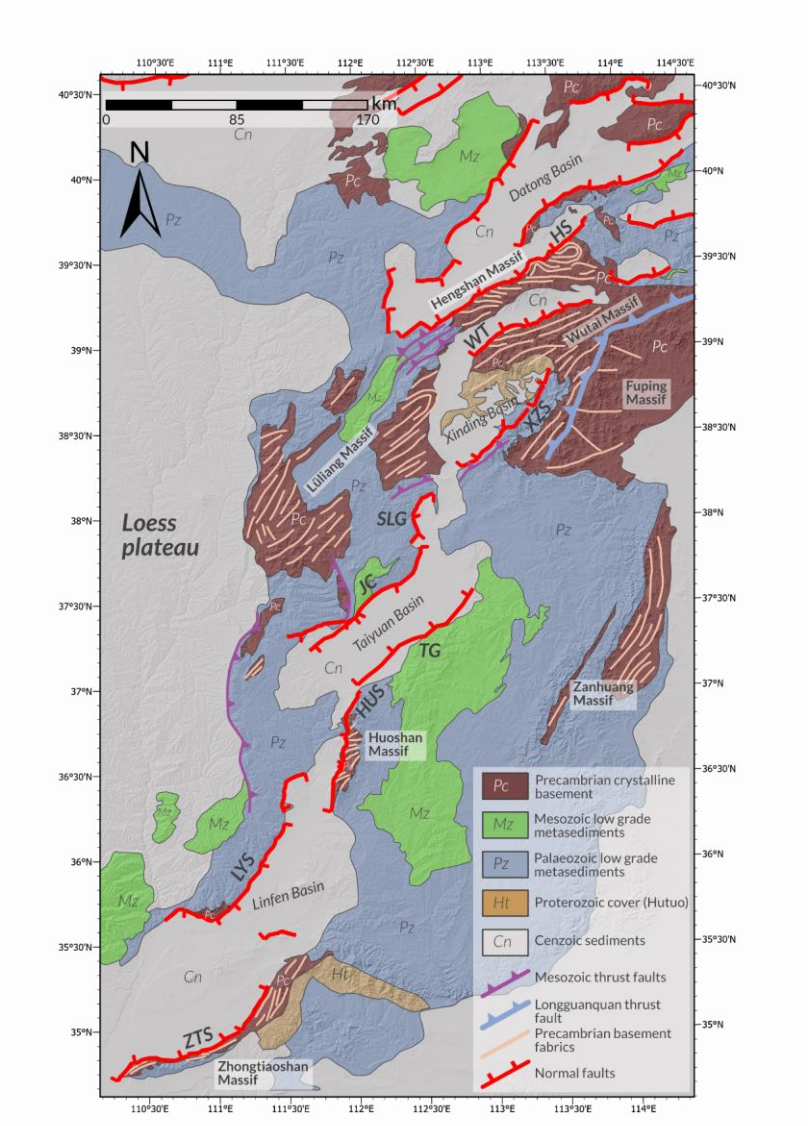
km
0
85
170
N
Loess plateau
Datong Basin
Hengshan Massif
HS
WT
Wutai Massif
Fuping Massif
Xinding Basin
XTS
Lüliang Massif
SLG
JC
Taiyuan Basin
TG
Zanhuang Massif
HUS
Huoshan Massif
LYS
Linfen Basin
ZTS
Zhongtiaoshan Massif
Pc Precambrian crystalline basement
Mz Mesozoic low grade metasediments
Pz Palaeozoic low grade metasediments
Ht Proterozoic cover (Hutuo)
Cn Cenzoic sediments
Mesozoic thrust faults
Longguanquan thrust fault
Precambrian basement fabrics
Normal faults

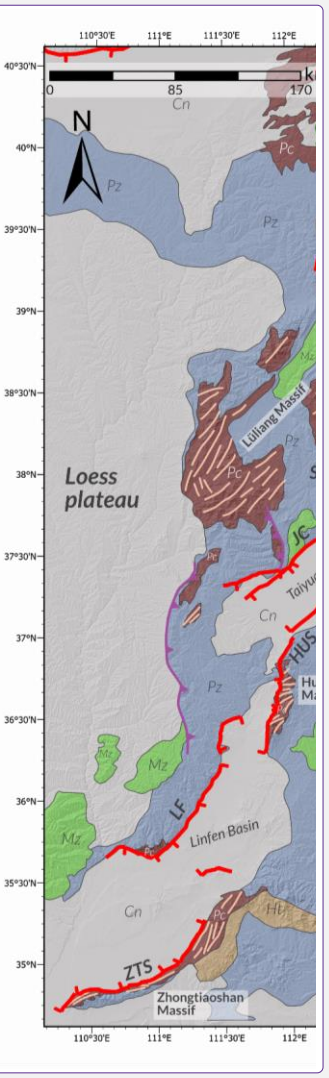
N
Loess plateau
Linfen Basin
LF
Zhongtiaoshan Massif
ZTS

Deleted:

Figure 3: Simplified geological map of the Shanxi Rift (modified from SBGMR, 1989 and Clinkscales et al., 2021) showing the main structures (Faure et al., 2007, Trap et al., 2007, Trap et al., 2009, Zhang et al., 2011; Clinkscales and Kapp, 2019). Main metamorphic fabrics are indicated in grey lines which are predominantly orientated NE-SW.

Since the Mesozoic, parts of the NCC have been removed by thermal erosion (Griffin et al., 1998; Menzies and Xu, 1998) and/or partial delamination (Gao et al., 2002; Gao et al., 2004), which is likely to be connected to the subduction of the palaeo-Pacific underneath East Asia (Menzies et al., 2007; Zhu et al., 2012). The eastern and western part of the NCC underwent a different evolution during the Mesozoic. The eastern part experienced compressive deformation from the Jurassic to Early Cretaceous (Davis et al., 2001), also regionally known as the Yanshanian Movement (Wong, 1927, Dong et al., 2015), which was less pronounced within the Western Block. However, Paleoproterozoic orogenic belts like the TNCO also recorded this widespread compressional event (Zhang et al., 2008; Zhang et al., 2011; Clinkscales and Kapp, 2019). Since the Early Cretaceous, the eastern NCC experienced extension, resulting in structures such as pull-apart basins, core complexes and associated voluminous magmatism (Zhu et al., 2012). Destruction of the cratonic lithosphere was limited to the eastern NCC, which resulted in Mesozoic magmatism almost exclusively affecting the eastern NCC (Zhu et al., 2012). Here, the North China Basin formed in the Eocene-Oligocene (Allen et al., 1997). This basin shows transtensional kinematics, which give it a resemblance to a giant pull-apart (Chen and Nabelek, 1988; Farangitakis et al., 2020). During the Paleogene, the western NCC experienced limited extension. The Shanxi Rift is one of a series of Neogene, narrow rifts which follow the trend of Precambrian orogenic belts within the NCC, developing around the Ordos Block (Shi et al., 2020).

The Shanxi Rift is a NE-SW trending rift system that consists of a series of left-stepping en-echelon basins (Zhang et al., 2003) (Fig. 2). The system is ~1000 km long and ~300 km wide and is bound to the north by the Yinshan-Yanshan Range and to the south by the Qinling Range (Fig.1). It is commonly believed to have initiated in the Late Miocene based on the oldest sediments found in the rift grabens - the Kouzhai Formation (Xu et al., 1993). The crust beneath the Shanxi Rift is ~32-39 km thick and is thinner in the basinal regions than adjacent to the Lüliang and Taihangshan highlands, which flank the rift to the west and east (Chen, 1987, Tang et al., 2010). The Shanxi Rift is characterized by a series of distinct rift basins that have either half-graben or graben geometries, separated by two topographically higher elevated areas, which have previously been called push-up swells but are referred to here as RIZs (Fig. 2) (Xu and Ma, 1992; Xu et al., 1993). The Linfen Basin to the south is separated by the Lingshi RIZ from the Taiyuan Basin, which is in turn separated from the Xinding Basin in the North by the Shilingguan RIZ. There are two main rivers that drain the Linfen-Taiyuan-Xinding basin system of the Shanxi Rift: The Hutuo River towards the east across the Xizhoushan Fault into the North China plain while the Fen River is diverted to the South where it drains into the Yellow River (Fig. 2), while the main drainage divide between the Fen and Hutuo River, is represented by the Shilingguan RIZ. The synrift thickness across the Shanxi Rift varies; While the Taiyuan basins has the thickest synrift sediment thickness of up to 3800m (Xu et al. 1993), the Xinding only contains up to a 1800m (Xu et al. 1993) and the Linfen basin contains up to 2200m of synrift fill (Su et al., 2023). The Shanxi Rift shows a widespread seismicity of M_w = 3-5 events on USGS and ISC records (Fig. 2), but the rift has produced infrequent but devastating earthquakes in historical time. The AD 1303 Hongdong Earthquake is believed to have been an M_W ~7.5 event (Xu et al., 2018) and is well-documented in Chinese

Deleted: destroyed
Deleted:)
Deleted: Eastern
Deleted: Western
Deleted: Eastern
Deleted: during
Deleted:)
Deleted:)
Deleted: record
Deleted: Eastern
Deleted: Eastern
Deleted: .
Deleted: has
Deleted: Western
Deleted: .
Deleted: 2a
Deleted: .
Deleted:
Deleted: draining
Deleted: East
Deleted: with
Deleted: these

historical writings. Shanxi Province itself is densely populated with 36.5 million inhabitants. Large cities like Taiyuan (5 million inhabitants), Linfen (4 million inhabitants) and Datong (3 million inhabitants) are close to active faults (Fig. 2) Constraining the exact extension direction and rate along extensional faults is difficult due to the Shanxi Rift's low extensional strain rate. Conducted research has been based on field-based fault slip measurements, GPS derived velocities and/or earthquake focal mechanisms to constrain the extension direction. Studies by Shen et al. (2000), He et al. (2003) and Middleton et al. (2017) constrain the extension direction in the Shanxi Rift to ~105°-165° and extension rate to ~ 0 - 6mm/year (Fig. 2). Other studies using field-based measurements (Shi et al., 2015a; Assie et al., 2022) propose a complex evolving strain field that has changed throughout the Cenozoic. According to these studies, NW-SE extension in the Mio-Pliocene initiated the rifting in Shanxi and was followed by NE-SW extension in the early Quaternary, leading to further subsidence. Theses authors suggest that the onset of the current NNW-SSE extension strain field started at 0.11 Ma and marked a shift from NW-SE extension to right lateral deformation in the Shanxi Rift, dated using faulted basalts in the Datong Basin (Shi et al., 2015a). Shi et al. (2015b) and Shi et al. (2015a) relate these changes in the strain field to growth of the Tibetan Plateau.

Deleted: .

Deleted: A variety of researchers have used

Deleted: between

Deleted: ° and

Deleted: as being between

Deleted: and

Deleted: developed

Deleted: of that age

3 Methods

3.1 Pre-Rift Architecture and Structural Mapping

We compiled a map of the structures in the Shanxi Rift (Fig. 3) by digitising Precambrian basement fabrics, Mesozoic and Precambrian thrust faults as well as Cenozoic active faults from published maps in ArcGIS Pro™. Additionally, we compiled published structural data from the Paleoproterozoic basement complexes to plot on stereonets (Fig. 4). In this study, we primarily focus on the influence of inherited structures in the Palaeoproterozoic basement on the evolution of the Shanxi Rift, therefore, if not specified otherwise, we refer to Palaeoproterozoic structures when discussing basement or inherited fabrics. To map the active fault structures, we identified linear breaks in the landscape on SRTM topographic data with 90 m resolution (https://lpdaac.usgs.gov/products/srtmgl3v003/) aided by slope and curvature attributes. This resolution is appropriate for the larger regional scale of this study and helped keep computing power demands manageable. We define active faults as linear, steep scarps (>20-30°) that offset Quaternary sediments, similar to the approach by Wedmore et al. (2022). Furthermore, we used topographic profiles across faults and geomorphological features such as steepened river channels and triangular facets along the fault scarp as features guiding our identification of active normal faults.

Deleted: , shear zones and

Deleted: .

Deleted: Figure 2 shows a topographic map and location map of the study area.…

Formatted: Font: Not Bold

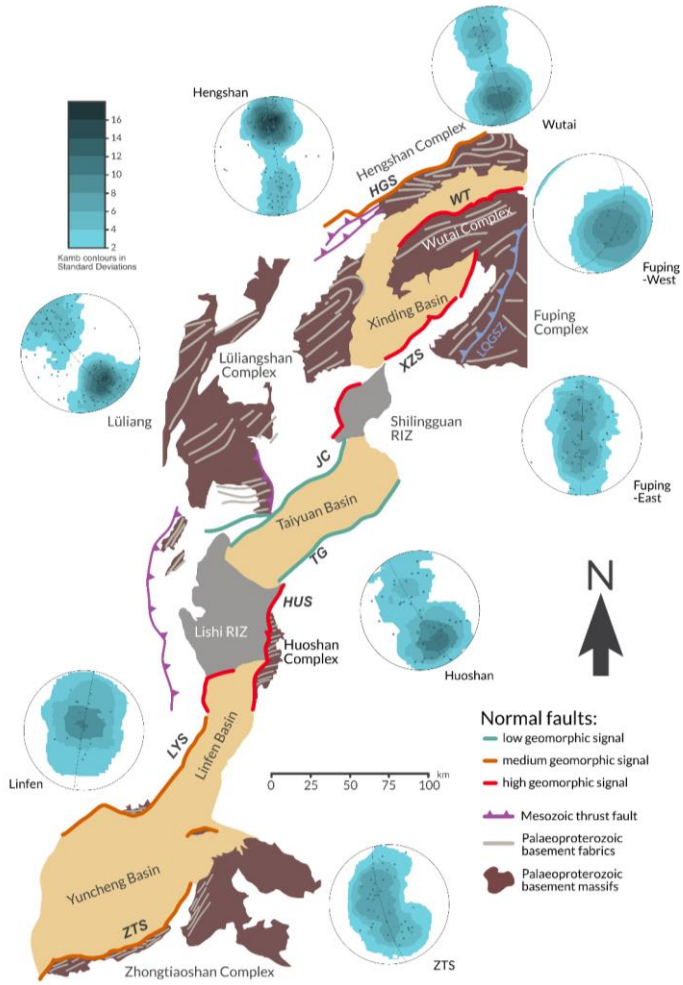

Figure 4: Schematic fault map of the Shanxi Rift with faults colour coded according to their geomorphic signal – compare with Table 1. Exposed basement of the TNCO in brown with the main structural trends highlighted in light grey. Stereonets of poles to planes (data from Trap et al., 2007; Trap et al., 2009a) show the structural grain of the main basement complexes. Most basement complexes show a NE-SW orientated grain, but it is more E-W in the North.

Moved (insertion) [3]

3.2 Geomorphic Indices

We used geomorphic indices to quantify the landscape response of the Shanxi Rift to tectonic drivers. We analysed the morphometric indices from 10873 1st order drainage basins located in the Shanxi Rift, extracted from the SRTM dataset using Topotoolbox2 Matlab scripts (Schwanghart and Scherler, 2014). We focused in this study on three geomorphic indices, 1) local relief (R_l) (Fig.5a), 2) the normalised channel steepness (k_{sn}) (Fig.5b) 3) the Hypsometric Integral (HI) (Figs. 5c, 6) and, as these proved to be the most helpful and discerning when evaluating the tectonic signals (Pérez-Peña et al., 2009; Gao et al., 2016; Obaid and Allen, 2019; Groves et al., 2020; Erbello et al., 2022). Using R, we also generated violin plots that visualise the distribution of values for each geomorphic index (Fig.7). The shape of the "violins" represents the distribution of values as the violin will be thicker the more data points sit at that range. Using these violin plots, we can also assess the impact of lithology on the geomorphic indices that enable us to compare the distribution of values per fault to the dominant footwall geology of the fault and assess if lithology is the principal factor determining the distribution.

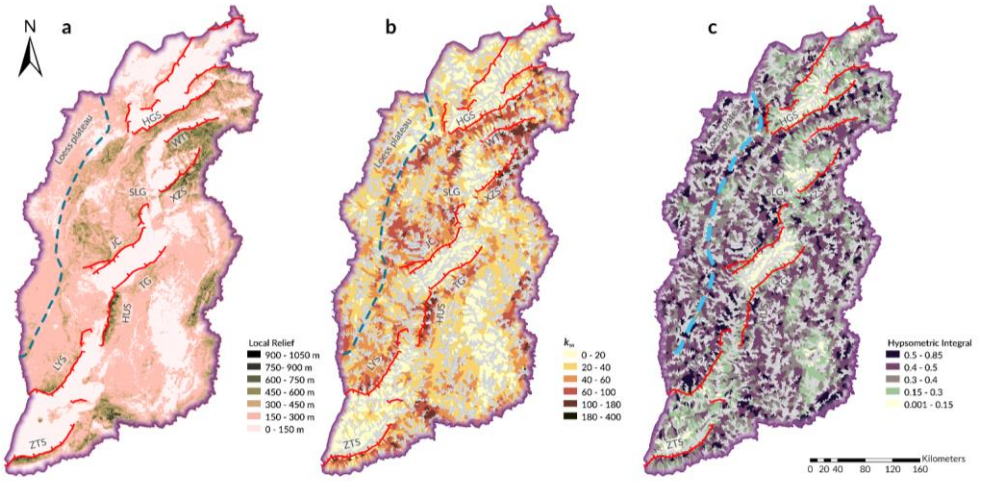

Figure 5: Geomorphic indices map of the Shanxi Rift. Major extensional faults shown in red, boundary of the Loess plateau indicated by dashed line a) Local relief map. Darker colours indicate higher relief regions. Local relief was calculated within a 1km circular radius. High relief is found especially in the northern Shanxi Rift in the footwalls of the Wutai and Xizhoushan faults as well as further south along the Huoshan and Zhongtiaoshan faults. Noticeably lower local relief values occur along the central Jiaocheng and Taigu faults. b) Mean normalised channel steepness (k_{sn}) calculated for 1st Strahler order basins. High values are commonly located in the footwalls of active faults, especially the Wutai, Xizhoushan and Huoshan faults. Low values are found in the lower lying basin regions. Central faults (Taigu and Jiaocheng) show noticeably less high k_{sn} basins than other faults. c) Hypsometric

Formatted: Font: Bold
Formatted: Justified, Line spacing: 1.5 lines
Deleted: ,
Deleted: Hypsometric Integral (HI) and, 3) the
Deleted: .
Deleted: to
Deleted: ¶
Moved (insertion) [4]
Moved (insertion) [5]
Moved (insertion) [6]

Integral (HI) calculated for 1st Strahler order basins. High values are commonly located in the footwalls of active faults, especially the Wutai, Linfen, Shilingguan and Huoshan faults. Low values are found in the lower lying basin regions.

(Abbreviations: HGS-Hengshan; WT-Wutai; XZS-Xizhoushan; SLG-Shilingguan; JC-Jiaocheng; TG-Taigu; HUS-Huoshan; LYS-Luoyunshan; ZTS-Zhongtiaoshan)

3.2.1 Local Relief (R_l)

Local relief is a commonly used measurement of the variation of topography over an area to analyse spatio-temporal tectonic trends (Ahnert, 1970; Schmidt and Montgomery, 1995; DiBiase et al., 2010). The relief R_l was calculated as the maximum difference in elevation E over; 1) a delineated drainage basin (S1) or 2) within a circular moving window with a 1 km radius:

$$R_l = E_{max} - E_{min} \quad (1)$$

where R_l is the local relief and E refers to elevation. High relief landscapes therefore show a higher variation of elevation over an area, which may indicate faster uplift rates. However, local relief is also influenced by lithology, high relief landscapes can also be the result of resistant lithologies with low erodibility.

3.2.2 Normalised Channel Steepness (k_{sn})

Normalised channel steepness (k_{sn}) is a frequently used topographic metric in tectonic geomorphology (DiBiase et al., 2010; Whittaker and Walker, 2015). For steady-state landscapes, meaning that rock uplift rates and river incision rates are at equilibrium, the channel slope S is defined as a power law function (Hack, 1957; Flint, 1974):

$$S = k_s A^{-\theta} \quad (2)$$

where A is the drainage area. The parameter k_s is the channel steepness index, and θ denotes the channel concavity index. (Snyder et al. 2000). In natural landscapes, its well known that variations in the best-fit for concavity index (θ) has a significant impact on estimates of k_s. To circumnavigate the problem, we used a reference concavity index of 0.45 (Wobus et al. 2006). This reference concavity index results in a dimensionless "normalised" channel steepness k_{sn}. Variations in k_{sn} along channel segments may be related to changes of the uplift rate of that region (Snyder et al., 2000; Whipple, 2004) with higher k_{sn} values often indicating higher uplift rates.

We used the TopoToolbox2 Matlab scripts (Schwanghart and Scherler, 2014) to extract the river profiles and calculate the normalised channel steepness from smoothed river profiles. This approach is built upon the method developed by Perron and Royden (2013) to analyse river profiles. We extracted streams with a drainage area of above 1 km^2 to avoid hillslope areas. Normalised channel steepness (k_{sn}) is commonly applied to stream networks to visualise knickpoints (variations in the slope of river channels) in rivers. In this study we used Topotoolbox2 to calculate the basin averaged k_{sn} values. This is achieved by calculating the mean of all k_{sn} values in each drainage basins. This makes it easier to compare the k_{sn} values to those for local relief and HI. The k_{sn} stream network map is available in the supplementary material (S2).

Deleted: spatiotemporal

Moved (insertion) [7]

Deleted: 3.2.2

Moved (insertion) [8]

Moved (insertion) [9]

Moved (insertion) [10]

Moved (insertion) [11]

3.2.3 Hypsometric Integral (HI)

The Hypsometric Integral (HI) was first used as a geomorphic index by Strahler (1952, 1957). It is a measurement of the distribution of elevation within an area. HI is derived as the integral of the hypsometric curve, which plots normalised elevation over normalised drainage area for each drainage basin. Fig. 6 illustrates the theory behind HI. The interpretation of the hypsometric curve assumes that topographically more youthful basins will have a convex-up shaped curve while more mature ones will have a more concave-up shape. If uplift outpaces erosion, there will be a greater range of elevation over an area, which results in a convex-up shaped curve and a high HI. Therefore, high HI values should coincide with rapidly uplifting areas (e.g., footwalls of active normal faults) (Hamdouni et al., 2008; Perez-Pena et al., 2009; Obaid and Allen, 2019; Groves et al., 2020; Erbello et al., 2022). HI may be influenced by other factors than tectonic uplift such as climate, lithology and basin shape and area. Lifton and Chase (1992) propose that at larger scale analysis (>1000km), tectonics will play have a larger effect than lithology, while at smaller scales, lithology can have a considerable impact. Masek et al. (1994) propose that climate can influence the hypsometry of an area. Several studies propose that basin shape and area influence the HI of a basin (Lifton and Chase, 1992; Masek et al. 1994; Hurtrez et al., 1999; Chen et al., 2003). However, Walcott and Summerfield (2008) analysed the basins of southern Africa and could find no impact of basin scale on HI. High HI regions may often be indicative of fast uplift rates but could also be related to other factors. Therefore, when analysing the tectonic implications of HI, it is important to be aware of these limitations. To mitigate the effect of lithology on our tectonic analysis, we also compare the HI distribution per fault with the predominant lithology of the fault's footwall using violin plots generated with R (Fig. 7c).

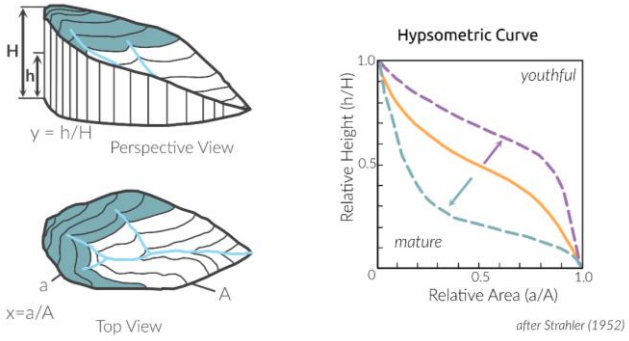

Figure 6: Schematic diagram explaining the concept of the Hypsometric Integral (after Strahler, 1952). Every drainage basin is dissected into elevation bands to determine a ratio of relative height over relative area. Concave curves indicate more youthful topography while convex shaped ones indicate more mature topography.

In this study, we calculated the HI per drainage basin (Obaid and Allen, 2019; Groves et al., 2020). The shape and size of drainage basins is controlled by tectonic and geological features. Therefore, drainage basins are more natural boundaries for

comparing areas of variable uplift and erosion rates than calculating HI with an arbitrary moving window. We calculated the hypsometric curves using QGIS 3.16 and derived the integral for each curve through an R script (Supplementary material X1).

Shanxi Rift Fault characteristics

Fault	Trend (in degrees)	Footwall lithology	Mean R_l	Mean HI	Mean k_{sn}	Geomorphic response	Orientation of inherited structures
Hengshan	57	Crystalline Basement	234	0.33	68	medium	E-W
Wutai	65	Crystalline Basement	367	0.37	79	high	NNE-SSW
Xizhoushan	50	Crystalline Basement	320	0.36	72	high	NE-SW
Shilingguan	5	Low-grade metasediments	217	0.4	57	high	NE-SW
Jiaocheng	48	Low-grade metasediments	193	0.32	39	low	NE-SW
Taigu	49	Low-grade metasediments	168	0.29	33	low	NE-SW
Huoshan	12	Crystalline Basement	301	0.36	68	high	NE-SW
Luoyunshan	38	Low-grade metasediments + Crystalline basement	219	0.38	47	medium	E-W
Zhongtiaoshan	72	Crystalline Basement	208	0.31	43	medium	NNE-SSW

Table 1: Summarising the Fault and their geomorphological response as well as their lithology and the orientation of the inherited fabrics in vicinity of the fault.

4 Results

4.1 Pre-rift structural architecture

The northern part of the Shanxi Rift is dominated by uplifted Paleoproterozoic basement massifs. The Hengshan, Lüliang, Wutai and Fuping massifs are exposed in the footwalls of major basin bounding faults (Figs. 3, 4). In the south, the footwalls are more commonly dominated by Mesozoic and Palaeozoic sedimentary rocks, with notable exceptions being the Huoshan and Zhongtiaoshan faults, which also expose Paleoproterozoic metamorphic basement at surface.

The general trend of most Paleoproterozoic structures is broadly NE-SW, which is sub-parallel to the active rift faults. In the northern basement massifs (Hengshan and Wutai), there is a subtle change to WNW-ESE-trends (Figs. 3, 4). The dip of these structures is variable due to folded nature of these rocks (Trap et al., 2007; Trap et al., 2009a; Clinkscales and Kapp, 2019). The dip of the fabric's changes from dipping towards and away from the faults along strike and the dip of the fabrics ranges from 25-85° (Trap et al., 2007; Trap et al., 2009a). The orientations also show plunging fold geometries in the basement massifs of the Hengshan and the Lüliangshan mountains (Stereonets Hengshan and Lüliang, Fig. 4). The Fuping Massif displays a considerable spread of basement fabric trends that can be split into two groups: fabrics trending NE-SW in the NW and fabrics with an NNW-SSE trend in the SE (Stereonets Fuping-West and Fuping-East, Fig. 4). These two regions are separated by the NE-SW trending Longguangquan thrust fault (marked as a blue thrust fault on Figs. 3 and 4), which most

Moved up [7]: Normalised Channel Steepness (k_{sn})¶
Normalised channel steepness (k_{sn}) is a frequently used topographic metric in tectonic geomorphology (DiBiase et al., 2010; Whittaker and Walker, 2015).

Moved up [8]: rock uplift rates and river incision rates are at equilibrium, the channel slope S is defined as a power law function (Hack, 1957; Flint, 1974):¶
$S = k_s A^{-\theta}$

Moved up [9]: where A is the drainage area. The parameter k_s is the channel steepness index, and θ denotes the channel concavity index. (Snyder et al. 2000). In natural landscapes, its well known that variations in the best-fit for concavity index (θ) has a significant impact on estimates of k_s. To circumnavigate the problem, we used a reference concavity index of 0.45 (Wobus et al. 2006).

Moved up [10]: reference concavity index results in a dimensionless "normalised" channel steepness k_{sn}. Variations in k_{sn} along channel segments may be related to changes of the uplift rate of that region (Snyder et al., 2000; Whipple, 2004) with higher k_{sn} values often indicating higher uplift rates.¶
We used the TopoToolbox2 Matlab scripts (Schwanghart and Scherler, 2014) to extract the river profiles and calculate the normalised channel steepness from smoothed river profiles. This approach is built upon the method developed by Perron and Royden (2013) to analyse river profiles. We extracted streams with a drainage area of above 1 km^2 to avoid hillslope areas. Normalised channel steepness (k_{sn}) is commonly applied to stream networks to visualise knickpoints (variations in the slope of river channels) in rivers.

Moved up [11]: we used Topotoolbox2 to calculate the basin averaged k_{sn} values. This is achieved by calculating the mean of all k_{sn} values in each drainage basins. This makes it easier to compare the k_{sn} values to those for local relief and HI. The k_{sn} stream network map is available in the supplementary material (S2). ¶

Deleted: 3.2.3

Deleted: For steady-state landscapes, meaning

Deleted: 2)¶

Deleted: Using this

Deleted: In this study

Deleted: Linfen

Deleted: Fig

Deleted: 5

Deleted:)

Deleted: Fig

Deleted: 5

Deleted:)

Deleted: 5

Deleted: 5

Deleted: Fig

Deleted: 5)

likely originated as a shallow-dipping thrust fault in the Paleoproterozoic (Trap et al., 2008). The basement fabrics in the NW-part and the Longguangquan thrust fault are parallel to the Xizhoushan Fault (Fig. 4 – stereonet Fuping-West). Further north, the Paleoproterozoic basement fabrics of the Wutai complex are orientated ENE-WSW, which is mirrored by the active normal Wutai Fault.

4.2 Relief

The local relief of the region (Fig. 5a) closely follows the overall topography of the region but emphasises certain features to make them easier to identify. Two areas of high local relief can be identified in the north and south of the Shanxi Rift.

In the northern region around the Wutai and the Xizhoushan faults, the footwalls of the prominent bounding faults are highly elevated (2500-3000 m) and show local relief values exceeding 1000 m. In the southern part of the Shanxi Rift, the Huoshan Fault to the south also shows high local relief (>1000 m) in the footwall close to the bounding fault. These high relief faults in Shanxi show consistently high local relief values along their fault traces whereas the Zhongtiaoshan Fault has high local relief (>1000 m) along the western end of the fault but lower values towards the east.

The Shilingguan RIZ is characterised by shorter faults segments, and this region shows an elevated local relief of around 500 m. In some examples, in footwalls close to the main fault, the local relief exceeds 1000 m. This is seen where a broadly N-S trending fault and a broadly NE-SW trending fault intersect and link up. Further into the footwall of this fault, there are pockets of high (>1000 m) local relief, which are along the sides of the narrow gorge of the Fen River. Compared to faults in the North and South of the Shanxi Rift such as Huoshan, Zhongtiaoshan or Wutaishan, the elevation in this area is lower (~1500 m) but the local relief remains comparatively high (up to 1000 m). The two longest faults in the central region of the Shanxi Rift, which bound the Taiyuan Basin (Taigu and Jiaocheng faults), show a lower local relief response rarely exceeding 450 m, with elevation lying between 1500 and 2000 m. There are regions of medium-high values of local relief (450-750 m) away from active structures, for example in the Taihangshan mountains or to the west of the Lingshi RIZ.

The per fault distribution of relief values (Fig. 7a) shows a clear divide between faults. The faults which have Proterozoic basement rocks in the footwall (Huoshan, Xizhoushan, Zhongtiaoshan, Hengshan and Wutai) have a greater range of values often exceeding 400 m. This is especially pronounced for the Wutai and Xizhoushan faults. The Hengshan Fault is slightly different as its distribution of relief values is closer to the faults with Palaeozoic-Mesozoic sedimentary rocks in the footwall, having most of its values between 200-300m. The Zhongtiaoshan has a maximum at around 200m and therefore lower relief than the other faults but still has some values in the higher ranges, with maximum values of 600m. The faults with Palaeozoic and Mesozoic sedimentary rocks in the footwall (Shilingguan, Taigu, Jiaocheng and Linfen) have overall lower values and a smaller range of values. Most of their values lie between 200-300 m but their minimum values are below 100m. Shilingguan as the RIZ fault shows a similar maximum at 200-300m but is missing the low minimum values, resulting in a more compact distribution.

Deleted: .

Deleted: .

Moved up [3]: : Schematic fault map of the Shanxi Rift with faults colour coded according to their geomorphic signal – compare with Table 1. Exposed basement of the TNCO in brown with the main structural trends highlighted in light grey. Stereonets of poles to planes (data from Trap et al., 2007; Trap et al., 2009a) show the structural grain of the main basement complexes. Most basement complexes show a NE-SW orientated grain, but it is more E-W in the North. ¶
¶

Moved up [4]: Darker colours indicate higher relief regions. Local relief was calculated within a 1km circular radius. High relief is found especially in the northern Shanxi Rift in the footwalls of the Wutai and Xizhoushan faults as well as further south along the Huoshan and Zhongtiaoshan faults. Noticeably lower local relief values occur along the central Jiaocheng and Taigu faults. B

Moved up [5]:) Mean normalised channel steepness (k_{sn}) calculated for 1st Strahler order basins. High values are commonly located in the footwalls of active faults, especially the Wutai, Xizhoushan and Huoshan faults. Low values are found in the lower lying basin regions. Central faults (Taigu and Jiaocheng) show noticeably less high k_{sn} basins than other faults.

Moved up [6]:) Hypsometric Integral (HI) calculated for 1st Strahler order basins. High values are commonly located in the footwalls of active faults, especially the Wutai, Linfen, Shilingguan and Huoshan faults. Low values are found in the lower lying basin regions. ¶
(Abbreviations: HGS-Hengshan; WT-Wutai; XZS-Xizhoushan; SLG-Shilingguan; JC-Jiaocheng; TG-Taigu; HUS-Huoshan;

Deleted: Page Break ¶ ...

Deleted: ¶
¶ ...

Deleted: B

Deleted: C

Deleted: LF-Luoyunshan; ZTS-Zhongtiaoshan)¶

Deleted: 6a

Deleted: fault

Deleted: max

4.3 Normalised channel steepness (k_{sn})

Four regions show high basin averaged k_{sn} values (Fig. 5b): The Huoshan Fault, the Xizhoushan Fault (especially its northeastern part), the Wutai Fault and the Zhongtiaoshan Fault. These are the same regions that show high local relief (Fig. 5a and Section 4.2). Low values of ≤ 50 are rarely associated with obvious faults with a surface trace. The Jiaocheng and the Taigu faults footwalls have drainage basins with k_{sn} values between 50-85, which reflects the local relief response of these faults (Fig. 5a). The footwall of the fault bounding the Shilingguan RIZ shows elevated values. Notably the area where the broadly N-S and NE-SW trending faults link up show basins with k_{sn} ≥ 100. The k_{sn} value distribution (Fig. 7b) of the different faults shows a similar trend to the Relief as there is a separation between faults with different basement lithology. The faults with Proterozoic basement show much higher values reaching values of 200 while the faults with Palaeozoic-Mesozoic basement show narrower distributions rarely ≥ 100 and most values lying ≤ 50. The notable outliers here are the Hengshan Fault whose distribution again is more similar to the Palaeozoic-Mesozoic basement faults. Here the Shilingguan RIZ records higher values (> 100) than the other faults with Palaeozoic-Mesozoic basement footwalls and has a distribution more similar to the faults with Proterozoic basement footwalls like Wutai or Xizhoushan.

Deleted: 6b
Deleted: 6a
Deleted: less than
Deleted: 6a
Deleted: exceeding
Deleted: good
Deleted: exceeding
Deleted: below
Deleted: much
Deleted: faults

4.4 HI

While the local relief and the channel steepness show broadly similar distributions, the HI differs slightly and shows a more distributed pattern of high (>0.5) HI basins (Fig. 5c). The footwall blocks to the Wutai, Xizhoushan and Zhongtiaoshan faults show elevated responses but in contrast to the previously described geomorphic parameters they do not show the highest values. In the footwalls of these faults, HI values mostly range between 0.3-0.5 and only isolated regions show values > 0.5. The bounding fault of the Shilingguan RIZ has among the highest HI responses, with values often ≥ 0.5 and rarely ≤ 0.4. The Lingshi RIZ that is bounded by the Huoshan Fault also shows elevated values compared to the surrounding basins, due to its overall higher elevation and dissected topography. These high HI values match spatially with the high local relief and k_{sn} values. Therefore, the Shilingguan RIZ and Huoshan Fault have consistently higher values compared to the Wutai, Zhongtiaoshan or Xizhoushan footwalls. The Luoyunshan fault adjacent to the Lingshi RIZ also shows elevated HI basins (>0.5), especially towards the southern end where it shows a distinct fault bend, however these high HI values are not matched to the same degree by local relief and k_{sn} (Section 4.2/3). The Taigu fault has lower HI values (≤ 0.4), matching the low values for channel steepness and local relief. While the Jiaocheng fault has a greater spread with low values basins (0.2 – 0.4) but also higher HI value basins (0.5 – 0.85), especially towards the northeast of the fault as it approaches the Shilingguan RIZ.

Deleted: showed
Deleted: 6c
Deleted: go above
Deleted: exceeding
Deleted: below
Deleted: Linfen
Deleted: (below

High value HI basins (> 0.5) are also found in regions away from the active normal faults that showed no recent tectonic activity. High values are observed to the west of the Shanxi Rift in the Loess Plateau on the western edge of the HI map. (Fig. 5c). Similar to the relief and the channel steepness, high values are also observed in high elevation regions further away from

Deleted: 6c)

mapped active faults. These commonly correspond to known thrust faults or other contractional structures (Fig. 3) (SBRGM, 1989) which were last active in the Mesozoic and created relict topography.

The HI value distribution (Fig. 7c) differs from the previous two geomorphic indices significantly as a clear separation based on lithology/footwall age is not obvious anymore and the patterns are more dispersed. The general trend still appears that faults with Proterozoic basements have slightly higher values (~0.5), however the Zhongtiaoshan Fault while reaching very high HI values has most values sitting at 0.4, which is below the other faults with Proterozoic footwalls and closer to faults with Palaeozoic-Mesozoic sedimentary rocks in the footwall. Amongst these faults, the Luoyunshan and Shilingguan faults show higher values than Taigu and Jiaocheng faults. Overall, the Shilingguan and Huoshan faults within the RIZs record the highest values but they are not significantly elevated over for example the Wutai or Luoyunshan faults.

Deleted: fault

Deleted: Within

Deleted: Linfen

Deleted: fault

Deleted: the other two faults (

Deleted:).

Deleted: :

Deleted: Linfen

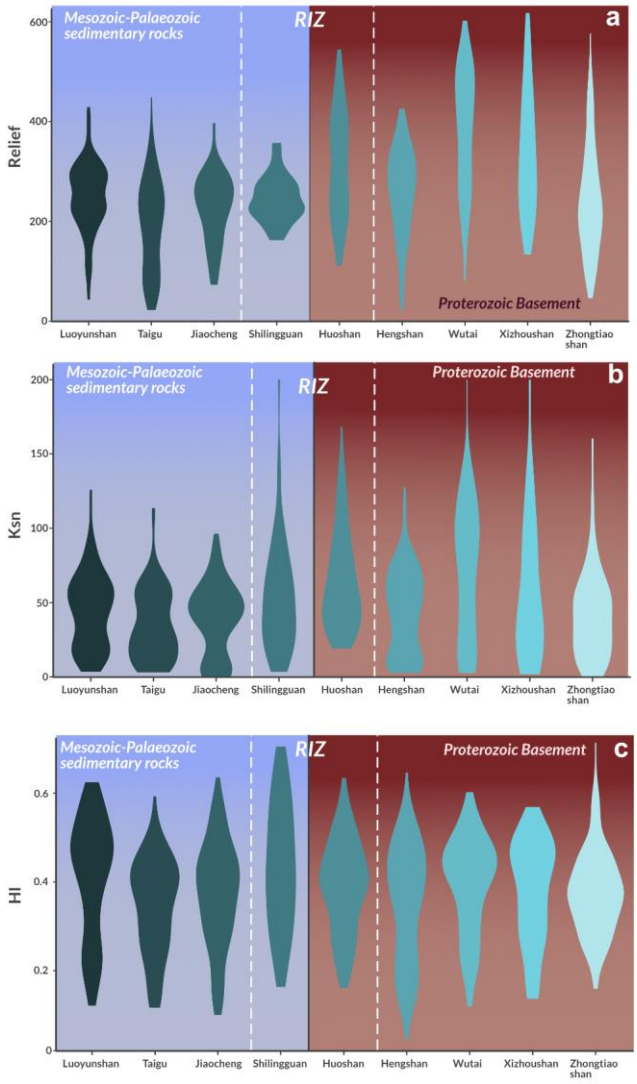
Mesozoic-Palaeozoic sedimentary rocks
RIZ
Proterozoic Basement
a
b
c
Relief
Ksn
HI
Luoyunshan
Taigu
Jiaocheng
Shilingguan
Huoshan
Hengshan
Wutai
Xizhoushan
Zhongtiaoshan

Deleted:

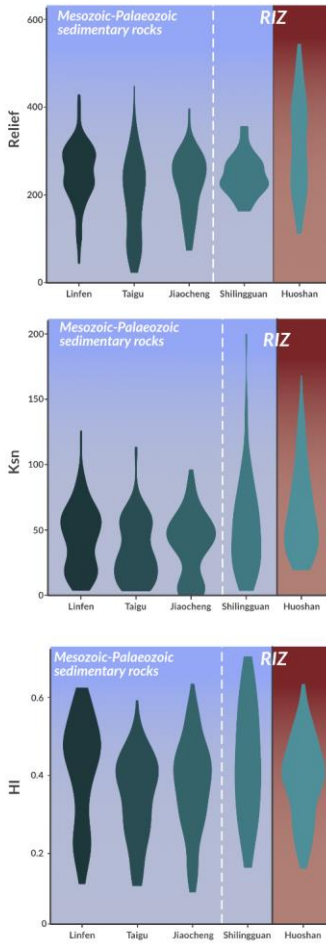
Mesozoic-Palaeozoic sedimentary rocks
RIZ
Relief
Ksn
HI
Linfen
Taigu
Jiaocheng
Shilingguan
Huoshan

Figure 7: Violin plots showing the distribution of geomorphic values for each fault. Background shows the dominant footwall composition of the faults with RIZ faults plotted in the middle. a) Local Relief. Clear separation of faults with high values all having Proterozoic basement-dominated footwalls. b) k_{sn} values showing a similar separation to the mean relief. c) HI values show more distributed values. RIZ tend to have high geomorphic values (see main text for more discussion on this)

Deleted: A)

Deleted: B

Deleted: C

5 Discussion

The quantitative analysis of the geomorphic response of the main rift faults has shown that the Wutai, Xizhoushan, Shilingguan and Huoshan faults show the highest geomorphic response (Fig.7; Table 1), they are classified by high HI (mean HI > 0.35), k_{sn} (mean k_{sn} >60) and R_l values (mean R_l > 250). Of those the Shilingguan and Huoshan faults are located within the RIZs and exhibit N-S as well as NE-SW trending fault segments. The Taigu and Jiaocheng faults that have the lowest geomorphic responses and show low values for all three geomorphic indices (mean HI < 0.3; mean k_{sn} < *40;* mean R_l < 200). In between these two groups are the Hengshan, Zhongtiaoshan and Luoyunshan faults, described as medium geomorphic response in Table 1. In the following we will discuss the significance of these results and discuss the possible influence of the pre-existing structures described in section 4.1.

5.1 Lithology dependence of geomorphic indices

The distribution of geomorphic indices for each fault shows significant differences (Fig. 7). Geomorphic response may be influenced by climate, lithology, and tectonics. The climate across Shanxi is continental and shows broadly little variation in precipitation (supplementary material S3; Fick and Hijmans, 2017) across the study region, which makes the differences in geomorphology between faults unlikely to be controlled by the climate. The lithology in Shanxi is more variable, as seen in Figure 3. The various lithologies can be divided into two main groups that differ in rock strength and erodibility. There are Precambrian crystalline rocks, which include Archean Tonalite–trondhjemite–granodiorite complexes, high-grade metamorphic rocks, and post-orogenic granites, which are all part of the TNCO (Trap et al., 2012), and the low-grade metasediments units, which include low grade clastic metasediments and carbonates from the Palaeozoic-Mesozoic (SBRGM, 1989). Here, we evaluate how these differences in lithology may have impacted the geomorphic response.

Deleted: .

Deleted:)

Local relief and k_{sn} (Figs. 5a, b) show the highest values where crystalline basement lithologies are exposed in the fault footwall. Faults with high mean local relief values (>300m) have "strong" crystalline basement in their footwalls (e.g., Huoshan, Wutai, and Zhongtiaoshan faults) or are directly adjacent to these (e.g., Xizhoushan Fault), while low values (~<200 m) are found in the faults with Palaeozoic-Mesozoic rocks in their footwalls (e.g., Taigu and Jiaocheng faults). HI (Fig. 5c) does not show the same bimodal distribution between faults with different footwall lithologies. The highest HI values correspond to faults with both Proterozoic basement footwall rocks (e.g., Huoshan, Wutai, and Xizhoushan faults) and Palaeozoic-Mesozoic footwall rocks (e.g., Shilingguan, Luoyunshan faults). Meanwhile, low HI values are also found for footwalls of both lithologies (e.g., Hengshan, Taigu, Jiaocheng, and Zhongtiaoshan faults). We can infer that the differences

Deleted: 6a

Deleted: .

Deleted: 6c

Deleted: Linfen

Deleted: and

in HI values between these fault blocks are not likely to be caused by lithology but rather by their tectonic history. This suggests that HI may be a more robust geomorphic index for analysing tectonic activity than relief or k_{sn} because it is less influenced by lithology. Our finding that HI is not primarily influenced by lithology agrees with previous studies (Obaid and Allen, 2019; Groves et al. 2020). High HI values are often correlated with high uplift rates, especially in regions with variable uplift rates, higher HI values are found in regions of higher uplift (Hurtrez et al. 1999). Therefore, the high HI values found in the footwalls of the Huoshan, Wutai, Xizhoushan and Shilingguan faults indicate that these footwalls have been uplifted the most rapidly.

To the western edge of the Shanxi Rift is a region of medium-high HI basins that do not correlate with mapped active faults. This is likely due to the landscape that typifies the Loess Plateau west of the Shanxi Rift. The Loess Plateau is unconsolidated wind-blown sediment that is prone to dramatic erosion, creating deep gullies and ridges, which can lead to high HI values. The Loess Plateau formed in the Pleistocene and its linear ridges and gullies have been carved out by aeolian and fluvial forces (Kapp et al. 2015), therefore the high response of the Loess Plateau is related to young landscapes sculpted by surface processes rather than tectonic forces. This does not detract from the main statement that HI is less influenced by lithology, as the Loess Plateau is an extreme case of unconsolidated sediment, as opposed to the main groups of low-grade metasediments and Palaeoproterozoic crystalline rocks. However, it does highlight that the HI response is sensitive to the presence of Loess. When using HI to evaluate the tectonic response of an area partially covered by Loess, it must be considered that Loess covered areas may show anomalously high HI values.

The dependence of some geomorphic indices on lithology is observed in many other areas worldwide and highlights the importance of considering the local geology for interpreting the relevance of geomorphic indices (Wobus et al. 2006; Kirby and Whipple, 2012). However, by comparing different faults with similar basement geology, the lithological impact can be reduced as theoretically they should have a similar rock strength and erodibility. This enables us to compare the landscape response of these footwall uplifts to tectonics. In the Shanxi Rift, the footwall of the Huoshan Fault on average has higher values for geomorphic indices than other faults with Paleoproterozoic crystalline rocks in the footwall (Fig. 7). Comparing the response of faults with footwall exposures of low-grade metasediments rocks, it becomes evident that the main bounding fault of the Shilingguan fault has a higher geomorphic response than the Jiaocheng, Luoyunshan and Taigu faults. The difference in geomorphic response between the Shilingguan fault and the other faults with low-grade metasediments in their footwalls is even more pronounced than among faults with Paleoproterozoic crystalline rocks in the basement. For example, the difference between the Huoshan and Hengshan faults is less stark than the difference between the Shilingguan Fault and the Jiaocheng Fault. It must also be noted that the Shilingguan fault shows higher HI and k_{sn} values than faults with "stronger" Paleoproterozoic crystalline rocks in their footwalls (Hengshan and Zhongtiaoshan). By comparing faults with similar footwall lithology, we can show that the difference in geomorphic response is not solely down to lithology and most likely has a tectonic origin.

Deleted: is

Deleted: fault

Deleted: to

Deleted: that creates

Deleted: are

Deleted: loess

Deleted: , therefore when evaluating

Deleted: this needs to

Deleted: accounted for

Deleted: around the world

Deleted: before

Deleted: for example

Deleted: fault

Deleted: .

Deleted: Linfen

Deleted: Here the

Deleted: comparing

Deleted: footwall where

Deleted: fault

Deleted: for example the

Deleted: or Wutai

Deleted: .

Deleted: a

Deleted: value

Deleted: ,

5.2 Implications for rift evolution, linkage and seismic hazard

Two significant zones in the evolution of the Shanxi Rift are the Shilingguan and Lingshi, that form between the major basins. Both zones are generally more elevated than the surrounding basins, making them potential sediment sources (Gawthorpe and Leeder, 2000), also shown by their patchy thin sediment fill compared to the major basins (Xu and Ma, 1992). The two RIZs differ in this geometrical organisation. The Shilingguan RIZ can be described as underlapping parallel divergent RIZ, while the Lingshi RIZ is an underlapping oblique convergent RIZ (compare with Fig.3 in Kolawole et al., 2021a). A potential third RIZ, the Hengshan RIZ, which separates the Datong and Xinding basins, can be proposed (Fig. 2). As an overlapping divergent RIZ is completely unbreached and therefore it will not be discussed at length in the following. The different RIZ stages come with distinct morphological responses and have relevance to the seismic hazard so in the following we classify the two RIZs in the Shanxi Rift based on the Kolawole et al. (2021a) classification scheme and assess the response of the geomorphic indices.

Deleted: two RIZs:

Deleted: which is

Deleted:), RIZs are classified on their geometrical organisation (rift segment faults are underlapping or overlapping, parallel, oblique or orthogonal).

Deleted: , the

Deleted: 2021). There is possibility of a

Deleted: . The Hengshan RIZ is

Moved up [1]: whether the RIZ is unbreached, partially breached, recently breached, or breached. This is assessed based on two observations: 1) Presence of a breaching fault that extends from one rift segment to the other segment

Moved up [2]:). Recently breached and breached RIZs have an established breaching fault and connect the drainage of two different rift segments, but breached RIZs shows less topography due to increased subsidence during the longer time period since the RIZ was breached. Unbreached RIZs show no apparent structural connection and no drainage connection, while partially breached RIZs may have a breaching fault partially connecting the rift basins but the drainage integration has not occurred yet.

Deleted: and

Deleted: ,

Deleted: RIZs can also be classified on their evolution stage (from Kolawole et al. 2021) i.e.

Deleted: and 2) Presence of an established physical linkage of depositional environments of both rift segments (i.e. is the drainage between both segments connected

Deleted: 2021

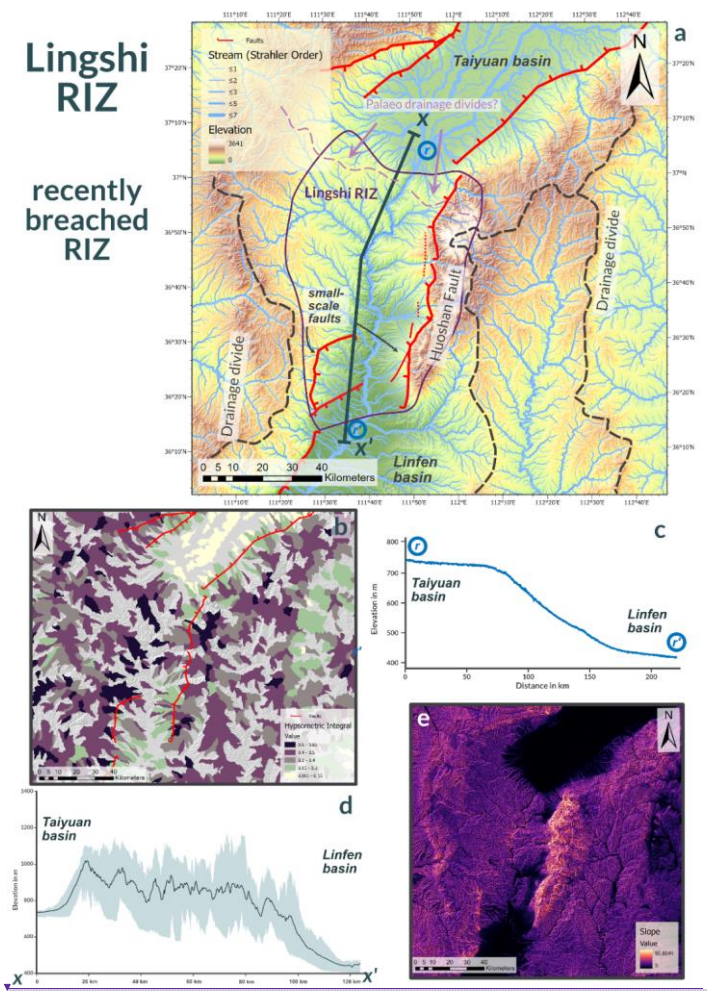

720 **Figure 8: a) Topographic map with drainage (weighted by stream order) showing the drainage divide and reorganisation happening at the Lingshi RIZ. b) HI map of the Lingshi RIZ, showing high values in the footwall of the Huoshan Fault but also in the hangingwall. c) Longitudinal river profile of the Upper Fen River showing the characteristic "down stepping" shape of river profiles across recently breached RIZs. d) Swath profile of the Lingshi RIZ, shaded area indicates maximum and minimum elevation in a 5km corridor along the line of section– line of section shown on 7a). e) Slope map of the Lingshi RIZ that shows very high values along the main border fault (Huoshan) but also clear distinct breaks in the SW.**

Deleted:

The Lingshi RIZ (Fig. 8) is the uplifted region between the Taiyuan and Linfen basins. The breaching fault, which in this case is the Huoshan Fault, is well developed and has established a physical connection between the Taiyuan and Linfen basins. The Huoshan Fault and other small-scale faults within the Lingshi RIZ are shorter, more segmented, and variably orientated compared to the faults of the major subbasins. These small-scale faults are more visible in the slope map (Fig. 8c), as sharp linear breaks. The footwall of the Huoshan fault shows high values of HI > 0.5 (Fig. 8b). However, the whole RIZ shows high values of HI, which are sometimes connected to smaller scale faults, highlighting the complexity and distribution of faulting in the RIZ. As noted in 5.1., the Loess Plateau can have a significant impact on the HI response of a region, therefore the high HI response in the Lingshi RIZ may in part be related to the degree of Loess coverage. However, the Loess is constrained to the hanging wall of the Huoshan Fault and therefore the high HI response in the Huoshan fault footwall is not influenced by Loess. The drainage of the Taiyuan and Linfen basins is connected across the Lingshi RIZ as the Fen River is flowing across it. The drainage was previously not connected as there are possible palaeo-drainage divides (in purple – Fig.8a), where tributaries of streams flow in separate directions. Li et al. (1998) proposed that during the early evolution of the Shanxi Rift in the Miocene and Pliocene, the basins were filled by isolated lakes and later, during the mid-Pleistocene, a fluvial connection was established. Hu et al. (2005) identified three lake terraces in the Taiyuan and Linfen basins, with the latest regression occurring at 0.13 Ma. Based on this, the integration and breaching across the Lingshi RIZ likely occurred in the Middle - Late Pleistocene. The swath profile of the RIZ and the longitudinal river profile (Figs. 8d, e) show the down stepping morphology that is commonly associated with recently breached RIZs may be a relic of the lake terraces prior to the fluvial connection being established. The Huoshan breaching fault (Huoshan) is well developed and has established a physical connection between the depositional systems of both basins, as the characteristic morphology of the Lingshi RIZ, we classify it as a recently breached RIZ.

The Shilingguan RIZ (Fig. 9) separates the Xinding Basin to the north and the Taiyuan Basin to the south. The breaching fault (Shilingguan Fault) is physically connected to the Jiaocheng fault but not to the Xizhoushan fault. The Shilingguan Fault itself appears to be segmented as seen by the various orientations of the fault segments (Fig. 9c). The topographic swath profile of the RIZ shows an outstanding topographic high (Fig. 9d). The footwall of the Shilingguan fault exhibits very high (>0.5) HI values and the Fen River in its footwall is highly sinuous but has high topography, relief, and steep slopes on either side, also known as an entrenched meander (Gardner, 1975; Harden, 1990). Combining all these observations indicates that this area of the Shanxi Rift has experienced recent uplift. The Shilingguan RIZ represents a drainage divide, with the Hutuo River, north of the RIZ is being deflected eastwards and draining across the Xizhoushan fault through the Taihang mountains into the North China Plain (Fig.2). In contrast, the Fen River flows from the NW and crosses the main breaching fault before draining towards the south into the Taiyuan basin. Windgaps (Fig. 9a) in the footwall of the Xizhoushan fault to the east show that possibly the drainage of the Upper Fen River once occurred across this RIZ from west to east before the initiation of the Shilingguan Fault and uplift of its footwall caused the diversion of the river to the south. As the depositional systems of the Xinding and Taiyuan

Deleted: southernmost RIZ connecting
Deleted: fault
Deleted: basin. (Kolawole et al., 2021).
Deleted: fault
Deleted:)
Deleted: in the excess of
Deleted:) however
Deleted: 4.1. loess
Deleted: loess
Deleted: loess
Deleted: loess
Deleted: basin are
Deleted: showing
Deleted: and
Deleted: As the
Deleted: which has connected
Deleted: as well
Deleted: fault
Deleted: the
Deleted: stand of the RIZ

basins are not connected across the RIZ, and the breaching fault has not established a full physical link, this RIZ represents a partially breached RIZ.

The different breaching stage of the Lingshi and Shilingguan RIZ may be related to their previously mentioned geometrical arrangement (Lingshi RIZ = underlapping oblique convergent RIZ; Shilingguan RIZ = underlapping parallel divergent RIZ), which led to earlier breaching of the Lingshi RIZ. The influence of initial geometry was shown by Kolawole et al. (2024) in a numerical model of the southern Malawi Rift, where the tip-to-tip arrangement of the Nsanje RIZ favoured rift coalescence compared to the overlapping divergent geometry of the Middle Shire RIZ. The convergent RIZ geometry of the Lingshi RIZ was beneficial for strain localisation and stress concentration at the fault tips of the surrounding basin bounding faults (Jiaocheng and Linfen), while the divergent geometry of the Shilingguan RIZ stalled rift coalescence. This in turn may also explain why the Hengshan RIZ is unbreached as it has an overlapping divergent geometry, which is unfavourable to stress concentration and rift coalescence. Breaching status of the RIZs increases towards the south, which may be controlled by the different RIZ geometries.

Deleted: ,

Deleted: (underlapping oblique convergent RIZ).

Deleted:)

Shilingguan RIZ

partially breached RIZ

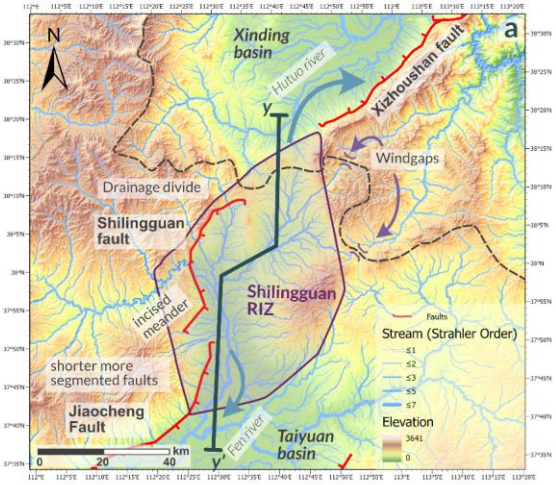

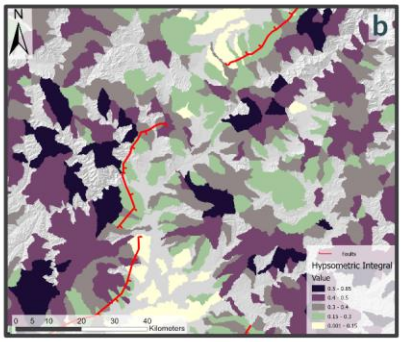

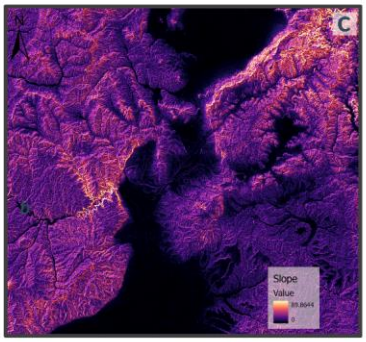

d

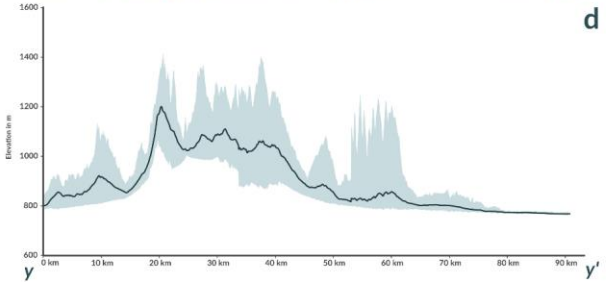

Figure 9: a) Topographic map with streams (weighted by stream order) showing the drainage divide and reorganisation happening at the Shilingguan RIZ. b) HI map of the Shilingguan RIZ, showing the high values in the footwall of the main faults, especially in the Shilingguan fault footwall where the high slope values are found. c) Slope map of the Shilingguan RIZ. High slope values are closely associated with the main faults but can also be seen along the steep sides of the meandering rivers in both the footwall of the Xizhoushan Fault and the Shilingguan Fault. d) Swath profile of the Shilingguan RIZ, shaded area indicates maximum and minimum elevation in a 5km corridor along the line of section – line of section shown in 8a)

Geomorphic evidence shows that the RIZ are currently the most active regions of faulting and reorganisation, as breaching faults of the RIZs (Huoshan and Shilingguan faults) show consistently high geomorphic values (Table 1; Fig. 7). They also show major changes in fault strike compared to the NE-SW trending basins (Figs. 8 and 9). Most faults in the RIZs do not strike NE-SW but show more distributed patterns of N-S and NE-SW striking faults. Commonly an overall "zig-zag pattern" forms, with fault segments of variable direction. Faults oblique to the general extension direction commonly form at the intersection points between major faults (Figs. 2, 8 and 9). Hodge et al. (2018a) show in models that Coulomb stress changes along the tips of established faults lead to the formation of new off-axis trending faults, with the geometry of these dependent on the lateral separation and amount of under- or overlap of the interacting faults. This process is common in other rift basins across the world (Maerten, 2000; Morley, 2010) and is similar to observations of faults in the RIZs of Shanxi. The N-S striking fault segments in the RIZs show overall higher geomorphic index values compared to the NE-SW trending faults of the sub-basins, suggesting they are more tectonically active as the active deformation is focused along zones of active linkage. The morphology of the N-S faults in the RIZs suggest that they are younger faults, which are still early in the reorganisation phase, as they are shorter, more segmented, and often show lower topographic offset (Fig.8, 9). Morphologically more mature NE-SW striking basin bounding faults have lower geomorphic index values than the faults in the RIZs, but can also show high values, especially in the case of the Wutai and Xizhoushan faults (Figs. 5 and 7). In the Shanxi Rift, faults of all orientations may show high activity levels, however faults in the RIZs show the highest activity. This activity pattern is consistent with an overall stable extension direction (Middleton et al. 2017), where all faults remain possibly active, but activity is concentrated in the linkage zones.

RIZs often experience high seismic activity due to increased strain along the tips of established basin bounding faults that progressively link across the RIZs. This was observed at the tips of the Rukwa Rift and the Rukwa-Tanganyika RIZ by Kolawole et al. (2021) and Kolawole et al. (2024), as well as for the Turkana Rift (Musila et al., 2023). The breaching faults in the RIZ could have a buffering effect on the NE-SW trending faults of the main sub-basins, as the overall strain accommodated across the Shanxi Rift is concentrated on the breaching faults in the RIZs, therefore the longer NE-SW trending faults accommodate overall less strain. Increased strain rate on faults post linkage has been shown to occur both in a theoretical framework (Cowie et al., 2005) and in natural examples such as the Whakatne Graben, NZ (Taylor, 2004). The heightened activity at these RIZs is not only shown by geomorphology but also by seismicity: Chen et al. (2021) processed receiver function data that show cluster of earthquakes at or near the Lingshi and Shilingguan RIZs, while events in the individual subbasins are more distributed. The ISC catalogue (Storchak et al., 2013; 2015; Di Giacomo et al., 2018) covering earthquakes

Deleted: .
Deleted: Figure
Deleted: Fig. 7 and
Deleted: .
Deleted: .
Deleted: .
Deleted: the idea of
Deleted:)
Deleted: increased
Deleted:)
Deleted: theory
Deleted: .
Deleted: shows
Deleted: both above-mentioned

occurring between 1907 and 2022 (Fig.2) show similar clusters around the RIZs, although the cluster around the Shilingguan RIZ is more pronounced. The faults in the Shilingguan RIZ are comparatively short and segmented (10-20km), this might limit the occurrence of large magnitude earthquakes along their trace. However, the Huoshan Fault, the breaching fault of the Lingshi RIZ, is equally segmented (Fig. 7a) with segments 20-30km in length and has shown to be the site of major historic earthquakes. The historic Hongdong Earthquake (M_w 7.2-7.6) in 1303 CE was caused by slip on the Huoshan Fault (Xu et al. 2018) and had an estimated rupture length of 98 km, which shows that multiple segments can link up during seismic slip to generate larger magnitude events. The Shanxi Rift is a low strain rate region, meaning major earthquakes are infrequent but potentially devastating as evidenced by the Hongdong 1303 event (Xu et al. 2018). Overall, the NE-SW trending faults, which are longer but potentially less active might be capable of generating larger but less frequent events (Scholz et al. 1982; Leonard, 2010), while the more segmented faults in the RIZs could produce more frequent yet smaller magnitude earthquakes.

Deleted: RIZ

Deleted: their ability to generate

Deleted: .

Deleted: Piedmont

Deleted: Piedmont fault

Deleted: 98km

Deleted: more infrequent

5.3 The role of inheritance in the Shanxi Rift – crust or mantle control?

Most continental rifts are influenced by inherited structures that are either reactivated (Daly et al., 1989; Wheeler and Karson et al., 1989; Holdsworth et al., 2001; Kinabo et al., 2008; Phillips et al., 2016; Wedmore et al., 2020; Kolawole et al., 2021b) or reorientate the rift scale strain field in local areas (Morley, 2010; Philippon et al. 2015; Kolawole et al., 2018; Samsu et al., 2023). The Shanxi Rift exploited rheological weaknesses during its formation at the rift scale (TNCO) and on smaller individual fault scales. At first order, the spatial relationship between the Shanxi Rift and the TNCO is obvious (Fig. 1). The Shanxi Rift is directly superimposed on the Paleoproterozoic orogen (Xu et al., 1993). The TNCO acted as a rheological weakness in comparison to the adjacent stronger Western Block of the NCC and therefore the TNCO was exploited by the Shanxi Rift. Orogenic belts behaving as weak zones for nucleating rifts is a common feature (i.e. East Africa (Rosendahl, 1987; Morley, 1988; Daly et al., 1989; Ring, 1994), and Baikal (Petit et al., 1996)). In the Shanxi Rift, faults often define the edges of Paleoproterozoic basement complexes and expose these at the surface by footwall uplift (e.g., Wutai, Hengshan, Xizhoushan, Zhongtiaoshan). Some of the rift faults do not contain Precambrian crystalline rocks in the footwall, but for example the Jiaocheng and Taigu faults in the direct vicinity of the crystalline Lüliangshan and Taihangshan massifs (~ 50 km distance). Basement complexes, such as the Huoshan, Fuping or Lüliangshan, are also cored by Precambrian granitic plutons, which formed as late orogenic intrusions during the TNCO development. These stronger more buoyant granitic blocks may have been more resistant to deformation hence the rift faults preferentially formed along the pluton margins and are uplifted within the fault footwall. This is similar to observations from offshore New Zealand (Phillips and McCaffrey, 2019; Phillips et al. 2023) or Carboniferous rift systems of the United Kingdom (Fraser and Gawthorpe, 1990; Howell et al., 2020).

Deleted: 2021

Deleted: suggestion

Deleted:) or

Deleted: -

Deleted:).

Deleted: .

Deleted: massif (about 50km

Deleted: formation

The similar trends of ancient pre-existing structures and active extensional faults show that the Paleoproterozoic fabrics of the TNCO potentially influence the orientation of the active faults of the Shanxi Graben. Major NE-SW trending basin bounding faults in the Shanxi Rift (Wutai, Xizhoushan, Taigu, Jiaocheng, and Zhongtiaoshan faults) are generally parallel to inherited NE-SW (45-55°) trending Paleoproterozoic basement fabrics (Fig. 4). The Wutai and Zhongtiaoshan faults all strike ENE-

Deleted: 5)

WSW (60-70°), matching the trend of the inherited structures in the footwall (Fig. 4). Therefore, it is likely that crustal structures influenced the orientation of these faults. The Hengshan fault locally trends parallel to the basement fabrics but often strikes obliquely and cuts across some of the shallow basement fabrics observed at surface (Fig. 4). It is possible that it locally exploits the shallow basement fabrics while following the trend of a deeper-seated weakness that is oblique to the shallow basement fabrics observed at surface, similar to the Bilila-Mtakataka Fault (Hodge et al. 2018b) in Malawi. The Xizhoushan fault follows the trend of the fabrics in the western part of the Fuping complex. There is a major crustal boundary running through the Fuping complex, which is known as the Longquanguang thrust (LGQT), a gently dipping thrust fault, according to Trap et al. (2012). To the southeast of the LGQT, there is a major change in trend of the Palaeoproterozoic fabrics to a generally NW-SE/E-W direction (compare stereonets of Fuping-West and Fuping-East on Fig. 4). The crustal structures of the eastern Fuping Block have no influence on the Xizhoushan fault (or any other fault in the Shanxi Rift), possibly because the LGQT represents a mechanical barrier. Based on their proximity and matching orientation, we speculate that the Xizhoushan fault may merge with the LQGT at depth. Merging of faults on shallower dipping structures has been observed by Phillips et al. (2016) in the North Sea. The >50 km long basin bounding faults of the Shanxi Rift nucleated along preferentially orientated inherited fabrics of the Palaeoproterozoic basement complexes, which may have aided with early fault nucleation similar to observations in other global rift systems (Phillips et al., 2016; Rotevatn et al., 2018; Heilman et al. 2019; Collanega et al., 2019; Vasconcelos et al., 2019; Ramos et al., 2022)

Faults in the RIZs show a more disconnected pattern (Figs. 8, 9), vary more in orientation (N-S and NE-SW), and are shorter (10-30km) than the large NE-SW trending basin bounding faults (up to 100km). Individual fault segments in the RIZs follow the broadly NE-SW trending crustal inherited fabric or cut across the fabric and strike N-S or NNE-SSW. As RIZ faults mature, segments link up and grow into one throughgoing "zig-zag" structure that cuts across pre-existing fabrics. This is especially visible on plan-view of the Huoshan Fault (Fig. 8). These "zig-zag" patterns in faults have been observed in offshore West Greenland (Peace et al., 2018, Schiffer et al., 2020), the North Sea (Henza et al. 2011; Henstra et al., 2015) and the main Ethiopian Rift (Moore and Davidson, 1978; Vetel and Le Gall, 2006; Corti et al., 2022; Lezzar et al., 2002; Corti, 2009; Hodge et al., 2018b). In the case of Greenland and Ethiopia, rifting was oblique to major basement shear zones, which lead to the formation of two sets of faults with some of them parallel to the extension direction and others parallel to the inherited structures. In the Shanxi Rift, the regional NW-SE extensional vector (Middleton et al. 2017) is likely perturbed around the RIZs due to interactions of the fault tips of the adjacent basin-bounding faults. Resulting into a strain field that would be oblique to the inherited structures. This leads to the formation of N-S trending faults that are perpendicular to the perturbed strain field and cut across the inherited basement fabrics, as well as NE-SW trending faults that follow the trend of pre-existing Proterozoic structures. Therefore, as the faults grow and coalesce across the RIZs, they will both cut across or locally exploit the inherited fabrics (Heilman et al., 2019; Kolawole et al. 2021b), resulting in the observed zig-zag fault pattern. Fault geometry may also be controlled by multiple levels of inheritance as observed by Wedmore et al. (2020) for the Thyolo Fault in Malawi and Hodge et al. (2018b) for the Bilila-Mtakataka Fault, where shallow level structures control the surface geometry

Deleted: of these faults.

Deleted: .

Deleted: fault (LGQF) which is

Deleted: ductile

Deleted: LGQF

Deleted: 5

Deleted: LGQF

Deleted: The

Deleted: LQGF

Deleted: ; however, this is mostly speculation based on their matching orientation and proximity

Deleted: (>50km)

Deleted:)

Deleted: long

Deleted: alternate between following

Deleted: , which broadly trends NE-SW, and cutting

Deleted: striking more

Deleted: has a "zig-zag" pattern that

Deleted: , this

Deleted: Piedmont

Deleted: various other rifts such as

Deleted: The resulting

Deleted: results in

Deleted: cutting

Deleted: following

Deleted: 2021

of the fault, but a deeper-seated weakness guides the overall orientation, which is oblique to the overall strain field. We consider that the NE-SW trending faults in the RIZs formed parallel to inherited fabrics at early stages and were linked up by N-S trending segments later. This behaviour is observed on the Norwegian Margin of the North Sea by Henstra et al. (2015) where rift faults from an early phase of rifting influenced the location and morphology of younger rift faults during a subsequent oblique phase of rifting. However, we did not find major morphological or geomorphological value differences between the N-S and NE-SW trending faults that would suggest a polyphase fault development, therefore it is possible that they are co-eval.

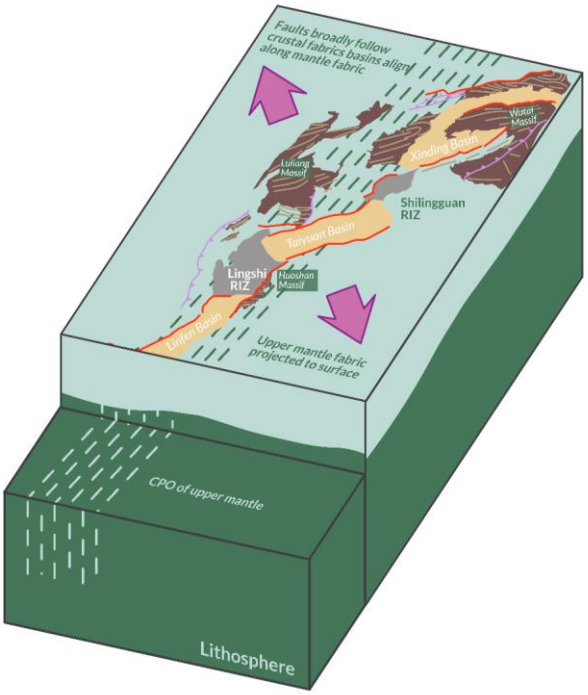

Figure 10: Schematic 3D diagram of the Shanxi Rift showing the proposed obliquity between mantle anisotropy and crustal inherited fabrics. Mantle anisotropy is defined by the suggested crystal preferred orientation (evidenced by shear wave splitting data (Zhao and Zheng, 2005)) in the upper mantle, that broadly trends N-S, while the crustal fabrics trend NE-SW. The Shanxi Rift basins are collated with a zone of aligned mantle fabric which is oblique to the principal extension direction (indicated as purple arrows). Individual basins and their bounding faults formed parallel to inherited crustal fabrics. This creates the characteristic en-echelon pattern of the Shanxi Rift.

Deleted: controls
Deleted: the possibility
Deleted: later
Deleted: was
Deleted: early
Deleted: a E-W orientated
Deleted: later
Deleted: , which was orientated obliquely to the early faults
Deleted: that one set formed earlier

The N-S and NE-SW trending faults in the RIZs can also be observed at the scale of the entire Shanxi Rift. The Shanxi Rift is an S-shaped en-echelon rift that follows a broad N-S trend with individual basins and their bounding-faults orientated NE-SW. While the TNCO broadly trends N-S/NNE-SSW (Fig. 1; Zhao et al., 2005), the individual crustal structures, such as major shear zones, thrust faults or fabrics, broadly trend NE-SW (Fig. 10). A broadly NNE-SSW to N-S trending anisotropy (0-15°) in the upper mantle of the Central Zone of the North China Craton is shown by shear wave splitting data from the upper mantle (Chen, 2010, Zhao and Zheng, 2005). The apparent obliquity between the trend of crustal structures and the upper mantle fabric shows that crustal inheritance and lithospheric inheritance may not share a common orientation, which is a common feature of many rift zones (Vauchez et al., 1997; Tomassi and Vauchez, 2001). Recent analogue modelling of oblique crustal and mantle fabrics by Zwaan et al. (2022) show similar patterns to those observed in the Shanxi Rift. Analogue models by Molnar et al. (2020) show that lithospheric weaknesses influence the rift trend, while oblique crustal structures segment the rift at a local scale. The difference in lithospheric and crustal structural trends could have either occurred during transpressional accretion of the TNCO, as proposed by Li et al. (2010) where subduction initially occurred along a N-S trend with later collision forming NE-SW trending structures. Alternatively, the polyorogenic event that formed the TNCO may have formed the obliquity between crustal and mantle structures, as the initial N-S trending TNCO was partially reworked by a collision of the Columbia supercontinent in the Palaeoproterozoic (Kusky & Li, 2003; Kusky et al. 2007; Santosh, 2010). However, the evolutionary history of the TNCO is debated and resolution of the exact timing of events is beyond the scope of this paper. Mesozoic compression across North China, commonly known as the Yanshanian orogeny (Zhang et al., 2008; Zhang et al., 2011; Clinkscales and Kapp, 2019) has also affected the Shanxi region and may have also caused further reworking of the TNCO and rotated the crustal fabrics to the present-day orientation. Solving the apparent obliquity between crustal and lithospheric trends of the TNCO is not resolvable in this study and would require further work on the kinematic evolution of the TNCO. The principal extension direction determined by Middleton et al. (2017) of 151° for the Shanxi Rift is roughly perpendicular to the inherited crustal structures, but oblique to the proposed broad upper mantle anisotropy, which resulted in the early rift basins exploiting the favourably orientated crustal fabrics, while the general trend of the rift is oblique to the extension direction along an upper mantle fabric that created a rheological weakness. This en-echelon arrangement of rift basins above a broad oblique deep seated weak zone has been shown in analogue models by Agostini et al., (2009), showing similar geometries as exhibited by the Shanxi Rift. However, we acknowledge that the observed mantle anisotropy may not be an inherited mantle fabric and could have formed during rifting (Gao et al., 1997; Kendall et al. 2006) and is aligned oblique to the rift (Tepp et al., 2018; Ebinger et al., 2024). Thus, the mantle fabric underlying Shanxi may be Cenozoic in age and has been formed during extensional deformation of North China as has been proposed previously (Chang et al., 2012). We emphasise that our interpretation that architecture of the Shanxi Rift is influenced by a crustal and mantle fabrics of the TNCO that are oblique to each other is speculative as the origin of the mantle anisotropy beneath the Shanxi Rift is unresolved. Yet, the apparent N-S trend of the TNCO, a roughly N-S trending mantle anisotropy and the NE-SW trending crustal fabrics may support the hypothesis that crust and mantle fabrics beneath the Shanxi Rift are oblique.

Deleted: trends of

Deleted: found at local scale

Deleted: are

Deleted: for

Deleted: or

Deleted: the

Deleted: modelling

Deleted: such

Deleted: while the

Deleted: that formed the TNCO formed

Deleted: fabrics. It may have also formed during later reworking by

Deleted: , where the

Deleted: which resulted in the formation of the E-W trending Inner Mongolia – North Hebei Orogen

Deleted: Determining the exact reason for

Deleted: .

Deleted: in the crust

Deleted: D'Agostini

Deleted: architecture

Deleted: .

Based on our geomorphic results, we propose a new model for the evolution of the Shanxi Rift that incorporates an heterogenous basement with inherited structures (Fig. 11), that can explain the evolution of the Shanxi Rift under a constant and simpler strain field, than a more variable strain field (Shi et al., 2015a; Shi et al., 2020; Assie et al., 2022). In our model, the extensional strain field trends NW-SE, which is consistent with previous estimations of the present-day extensional strain field using GPS or seismicity data (Middleton et al., 2017; Shen et al., 2000). However, locally the strain is reorientated either by inherited structures (i.e., Wutai and Zhongtiaoshan (Figs. 5, 8)) or interactions between basin-bounding faults that rotate the local strain field in the RIZs between them (Shilingguan and Lingshi) (Fig.11). This means that there is no specific set of faults that is favoured by changes of strain fields. Therefore, potentially all faults remain active, yet there are certain faults that are more active due to ongoing reorganisation and linkage in the RIZs. Faults established during early evolutionary stages along preferentially aligned NE-SW trending inherited structures and formed the major en-echelon Taiyuan, Xinding and Linfen basins along a N-S trending upper mantle structure (Fig. 10 and 11). As the faults and basins grew, they interacted and linked across almost unfaulted topographical high stands , the RIZs. These RIZs had a more complex faulting pattern as the interacting faults created a locally rotated strain field, which is oblique to the crustal structures and the regional strain field. This creates a "zig-zag geometry" as the shorter fault segments grow and coalesce. As linkage progresses, these RIZs link basins and establish physical and sedimentary system links. This linkage is currently ongoing, as represented by the only partially breached RIZ of Shilingguan.

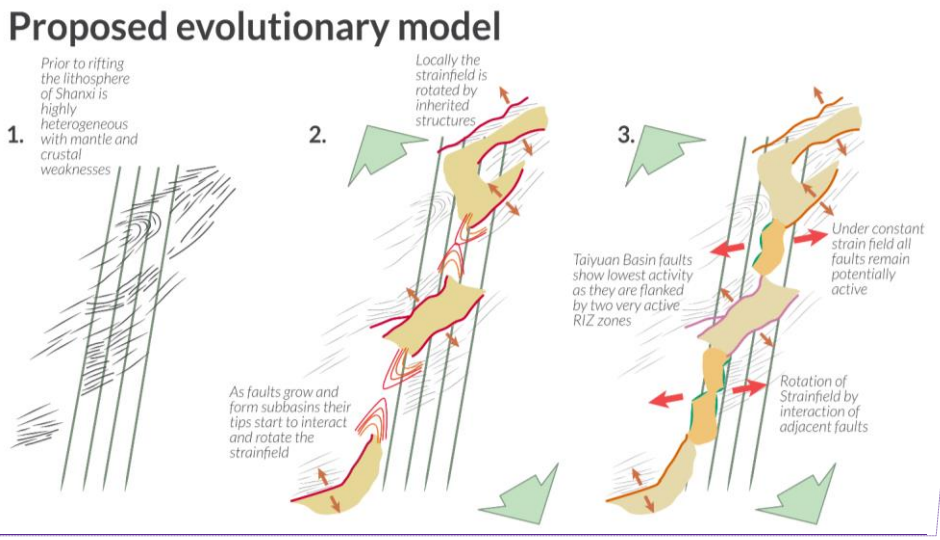

Fig. 11. The new proposed evolutionary model under a constant strain field that shows linkage of rift basins influenced by two levels of inheritance – crustal and mantle inheritance which result in oblique rifting and the creation of en-echelon array of basins. 1.

Deleted: We…ased on our geomorphic results, we propose a new model for the evolution of the Shanxi Rift that incorporates a…n heterogenous basement with inherited structures. This model is consistent with our geomorphic results…(Fig. 11) and…, that can explain the evolution of the Shanxi Rift under a constant and simpler strain field, making it simpler …han, frequent changes in the…a more variable strain field (Shi et al., 2015a; Shi et al., 2020; Assie et al., 2022). In our model, the extensional strain field trends NW-SE, which is consistent with previous estimations of the present-day extensional strain field using GPS or seismicity data (Middleton et al., 2017; Shen et al., 2000). However, locally the strain is reorientated either by inherited structures (i.e., Wutai and Zhongtiaoshan (Fig. 9…igs. 5, 8)) or interactions between basin-bounding faults that rotate the local strain field in the RIZs between them (Shilingguan and Lingshi) (Fig.11). This means that there is …

Deleted: . These…basins formed in an en-echelon arrangement…along a N-S trending upper mantle structure (Fig. 10 and 11). As the faults and basins grew, they started interacting…nteracted and linking…inked across almost unfaulted topographical high stands that saw less faulting and subsidence … the RIZs. These RIZs have…ad a more complex faulting pattern as the interacting faults create…reated a locally rotated strain field, which is oblique to the crustal structures and the regional strain field. This creates a "zig-zag geometry" as the shorter fault segments grow and coalesce. As linkage progresses, these RIZs link the different …asins and establish physical and sedimentary system links. This linkage is currently ongoing to the current day …

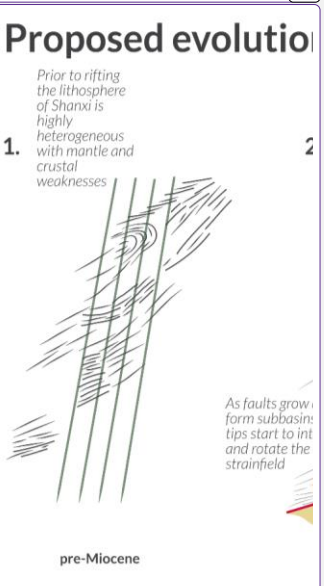

Deleted:

Deleted: **Crustal fabrics aid strain accommodation and influence geometry of linkage faults in the RIZs.**

Proposed pre-rift framework of NNE-SSW trending mantle fabric and NE-SW trending crustal fabrics. 2. Major basins form en-echelon along the NNE-SSW trending mantle fabric but form perpendicular to the extension direction (large green arrows) and along inherited crustal structures that locally reorientate the strain (smaller orange arrows). RIZs are created and major basin bounding faults start to reorientate the local strain field. 3. The RIZs are being breached and form smaller more segmented fault segments that are influenced by the locally reorientated strain field (red arrows) and inherited crustal structures.

6 Conclusions

We applied three different geomorphic indices (R_l, k_{sn} and HI) to analyse the fault distribution and the geometry and occurrence of rift interaction zones (RIZs) along the Shanxi Rift to discuss the distribution of tectonic activity and understand the role structural inheritance has played in its evolution and the seismic hazard posed by active faults within it. Based on our results we conclude the following:

1. Geomorphic indices are a powerful tool to evaluate the fault evolution and activity and the segmentation of the Shanxi Rift.
2. Our study shows that lithology has a strong influence on the overall geomorphic signal of faults, as those with Paleoproterozoic crystalline basement in their footwalls have overall higher geomorphic values compared to faults with Palaeozoic-Mesozoic metasediments in the footwalls. However, comparing faults with similar basement geology can circumvent this problem. We found that overall HI is less sensitive to these variations of lithology compared to Relief and k_{sn}. Therefore, HI may be more suited to evaluating the tectonic influence on landscapes.
3. Within the Shanxi Rift, the RIZs that link the well-developed large Xinding, Linfen and Taiyuan basins, are the most active zones and show most signs of active drainage reorganisation. This has major implications for seismic hazard assessments as it hints towards zones which show more complex and more active patterns of faulting due to the strain concentration in the RIZs, experiencing increased seismicity. Linkage of the basins seems to be progressing towards the north, as shown by the increasing breaching status of the RIZs towards the south, which is possibly controlled by their initial geometry.
4. Structural inheritance has played a key role in the evolution and segmentation of the Shanxi Rift. The collision of the two component blocks of the NCC created a lithospheric scale weak zone, the Trans-North China Orogen (TNCO), which preferentially accommodates strain. The individual sub-basins of the Shanxi Rift form en-echelon aligned along a broad N-S trend which coincides with an upper mantle anisotropy fabric – a lithospheric manifestation of the TNCO. The mantle anisotropy is oblique to the NW-SE extension direction, while the NE-SW trending crustal fabrics are perpendicular to the extension direction. Early rift faults nucleated along NE-SW orientated basement fabrics, establishing basins arranged along the inherited N-S trend. As the boundary faults grew, they began to interact and form RIZs. Within these RIZs, the crustal basement inheritance further influenced and segmented the breaching faults and aided linkage across the basins. The faults within the RIZs both follow and crosscut pre-existing fabrics in the crust, creating a "zig-zag pattern" of small, segmented faults that eventually link up into singular throughgoing fault

Deleted: the
Deleted: of the rift systems
Deleted: We have shown that geomorphic
Formatted: List Paragraph, Numbered + Level: 1 + Numbering Style: 1, 2, 3, … + Start at: 1 + Alignment: Left + Aligned at: 0.63 cm + Indent at: 1.27 cm
Deleted: The geomorphic analysis showed that in
Deleted: established
Deleted: basins, namely the
Deleted: these may experience
Deleted: the breaching status of the RIZ
Deleted:
Deleted: ,
Deleted: as it is more easily deformed than the surrounding cratonic area.
Deleted: align
Deleted: Inherited
Deleted: in the upper crust
Deleted: orientated NE-SW,
Deleted: regional extension direction. The
Deleted: is oblique to the assumed upper mantle inherited fabric which, causes the en-echelon pattern of individual rift basins
Deleted: them

zones. Therefore, structural inheritance of pre-existing Precambrian basement fabrics and a locally rotated stress field resulted in the complex pattern of faulting observed in the RIZs.

5. Our geomorphic study supports a constant strain field during the formation of the Shanxi Rift with minor changes of the extensional vector. We propose that the Shanxi Rift is a type-example of an oblique rift, with an observed pattern of faulting influenced by a postulated upper mantle anisotropy, crustal basement fabrics, as well as pre-existing faults.

Deleted: we now see in the RIZs. Thus, frequent changes of the extensional vector are not needed to explain the evolution of the Shanxi Rift as data is consistent with an evolution under a constant strain field. We propose that the Shanxi Rift is a type-example of an oblique rift that is influenced by an inheritance at different scales, as upper mantle, and crustal basement fabrics as well as pre-existing faults have influenced the pattern of faulting observed today.

Data availability

A geopackage of the GIS project with the associated raster files of the geomorphic indices is available on the Zenodo repository associated with this publication (https://doi.org/10.5281/zenodo.7317598, Phillips et al., 2022). They can be opened with QGIS. The R code for calculating the Hypsometric integral is available on GitHub: (https://github.com/MFroemchen/R_Hypsometry)

Deleted:) These

Author contributions

MF, KJWM, MBA, JVH and TBP conceptualised the study. MF undertook the geomorphic and structural analysis. MF prepared the manuscript and figures along with input from KJWM, MBA, JVH, and all other co-authors. All co-authors contributed to writing, revising, and preparing of the manuscript.

Competing interests

The contact author has declared that none of the authors has any competing interests.

Financial support

This research has been supported by the Natural Environment Research Council (grant no. NE/S007431/1).

References

Aanyu, K. and Koehn, D.: Influence of pre-existing fabrics on fault kinematics and rift geometry of interacting segments: Analogue models based on the Albertine Rift (Uganda), Western Branch-East African Rift System, Journal of African Earth Sciences, 59, 168–184, https://doi.org/10.1016/j.jafrearsci.2010.10.003, 2011.

Agostini, A., Corti, G., Zeoli, A., and Mulugeta, G.: Evolution, pattern, and partitioning of deformation during oblique continental rifting: Inferences from lithospheric-scale centrifuge models, Geochemistry, Geophysics, Geosystems, 10, https://doi.org/10.1029/2009GC002676, 2009.

Ahnert, F.: Functional relationships between denudation, relief, and uplift in large, mid-latitude drainage basins, American Jornal of Science, 268, 243–263, https://doi.org/10.2475/ajs.268.3.243, 1970.

Ai, S., Zheng, Y., He, L., and Song, M.: Joint inversion of ambient noise and earthquake data in the Trans-North China Orogen: On-going lithospheric modification and its impact on the Cenozoic continental rifting, Tectonophysics, 763, 73–85, https://doi.org/10.1016/j.tecto.2019.05.003, 2019.

Allen, M. B., Macdonald, D. I. M., Xun, Z., Vincent, S. J., and Brouet-Menzies, C.: Early Cenozoic two-phase extension and late Cenozoic thermal subsidence and inversion of the Bohai Basin, northern China, Marine and Petroleum Geology, 14, 951–972, https://doi.org/10.1016/S0264-8172(97)00027-5, 1997.

Assie, K. R., Wang, Y., Tranos, M. D., Ma, H., Kouamelan, K. S., Brantson, E. T., Zhou, L., and Ketchaya, Y. B.: Late Cenozoic faulting deformation of the Fanshi Basin (northern Shanxi rift, China), inferred from palaeostress analysis of mesoscale fault-slip data, Geological Magazine, 1–17, https://doi.org/10.1017/S0016756822000085, 2022.

Bonini, M., Souriot, T., Boccaletti, M., and Brun, J. P.: Successive orthogonal and oblique extension episodes in a rift zone: Laboratory experiments with application to the Ethiopian Rift, Tectonics, 16, 347–362, https://doi.org/10.1029/96TC03935, 1997.

Brune, S., Corti, G., and Ranalli, G.: Controls of inherited lithospheric heterogeneity on rift linkage: Numerical and analog models of interaction between the Kenyan and Ethiopian rifts across the Turkana depression, Tectonics, 36, 1767–1786, https://doi.org/10.1002/2017TC004739, 2017.

Bull, W. B. and McFadden, L. D.: Tectonic Geomorphology North and South of the Garlock Fault, California, in: Geomorphology in Arid Regions, Routledge, 1980.

Butler, R. W. H.: The influence of pre-existing basin structure on thrust system evolution in the Western Alps, SP, 44, 105–122, https://doi.org/10.1144/GSL.SP.1989.044.01.07, 1989.

Chang, L., Wang, C.-Y., and Ding, Z.: Upper mantle anisotropy beneath North China from shear wave splitting measurements, Tectonophysics, 522–523, 235–242, https://doi.org/10.1016/j.tecto.2011.12.009, 2012.

Chen, G.: On the geotectonic nature of the Fen-Wei rift system, Tectonophysics, 143, 217–223, https://doi.org/10.1016/0040-1951(87)90091-6, 1987.

Chen, L.: Concordant structural variations from the surface to the base of the upper mantle in the North China Craton and its tectonic implications, Lithos, 120, 96–115, https://doi.org/10.1016/j.lithos.2009.12.007, 2010.

Chen, W.-P. and Nábelek, J.: Seismogenic strike-slip faulting and the development of the North China Basin, Tectonics, 7, 975–989, https://doi.org/10.1029/TC007i005p00975, 1988.

Chen, Y., Chen, J., Li, S., Yu, Z., Liu, X., and Shen, X.: Variations of crustal thickness and average Vp/Vs ratio beneath the Shanxi Rift, North China, from receiver functions, Earth, Planets and Space, 73, 200, https://doi.org/10.1186/s40623-021-01528-8, 2021.

Chen, Y.-C., Sung, Q., and Cheng, K.-Y.: Along-strike variations of morphotectonic features in the Western Foothills of Taiwan: tectonic implications based on stream-gradient and hypsometric analysis, Geomorphology, 56, 109–137, https://doi.org/10.1016/S0169-555X(03)00059-X, 2003.

Clinkscales, C. and Kapp, P.: Structural style and kinematics of the Taihang-Luliangshan fold belt, North China: Implications for the Yanshanian orogeny, Lithosphere, 11, 767–783, https://doi.org/10.1130/L1096.1, 2019.

Clinkscales, C., Kapp, P., Thomson, S., Wang, H., Laskowski, A., Orme, D. A., and Pullen, A.: Regional exhumation and tectonic history of the Shanxi Rift and Taihangshan, North China, Tectonics, 40, e2020TC006416, 2021.

Collanega, L., Siuda, K., A.-L. Jackson, C., Bell, R. E., Coleman, A. J., Lenhart, A., Magee, C., and Breda, A.: Normal fault growth influenced by basement fabrics: The importance of preferential nucleation from pre-existing structures, Basin Research, 31, 659–687, https://doi.org/10.1111/bre.12327, 2019.

Corti, G.: Continental rift evolution: From rift initiation to incipient break-up in the Main Ethiopian Rift, East Africa, Earth-Science Reviews, 96, 1–53, https://doi.org/10.1016/j.earscirev.2009.06.005, 2009.

Corti, G., Iandelli, I., and Cerca, M.: Experimental modeling of rifting at craton margins, Geosphere, 9, 138–154, https://doi.org/10.1130/GES00863.1, 2013a.

Corti, G., Philippon, M., Sani, F., Keir, D., and Kidane, T.: Re-orientation of the extension direction and pure extensional faulting at oblique rift margins: comparison between the Main Ethiopian Rift and laboratory experiments, Terra Nova, 25, 396–404, https://doi.org/10.1111/ter.12049, 2013b.

Corti, G., Maestrelli, D., and Sani, F.: Large-to Local-Scale Control of Pre-Existing Structures on Continental Rifting: Examples From the Main Ethiopian Rift, East Africa, Frontiers in Earth Science, 10, 2022.

Cowie, P. A., Underhill, J. R., Behn, M. D., Lin, J., and Gill, C. E.: Spatio-temporal evolution of strain accumulation derived from multi-scale observations of Late Jurassic rifting in the northern North Sea: A critical test of models for lithospheric extension, Earth and Planetary Science Letters, 234, 401–419, https://doi.org/10.1016/j.epsl.2005.01.039, 2005.

Cox, R. T.: Analysis of drainage-basin symmetry as a rapid technique to identify areas of possible Quaternary tilt-block tectonics: An example from the Mississippi Embayment, GSA Bulletin, 106, 571–581, https://doi.org/10.1130/0016-7606(1994)106<0571:AODBSA>2.3.CO;2, 1994.

Crider, J. G. and Pollard, D. D.: Fault linkage: Three-dimensional mechanical interaction between echelon normal faults, Journal of Geophysical Research: Solid Earth, 103, 24373–24391, https://doi.org/10.1029/98JB01353, 1998.

Daly, M. C., Chorowicz, J., and Fairhead, J. D.: Rift basin evolution in Africa: the influence of reactivated steep basement shear zones, Geological Society, London, Special Publications, 44, 309–334, https://doi.org/10.1144/GSL.SP.1989.044.01.17, 1989.

Davis, G., Zheng, Y., Cong, W., Darby, B., Zhang, C., and Gehrels, G.: Mesozoic tectonic evolution of the Yanshan fold and thrust belt, with emphasis on Hebei and Liaoning provinces, northern China, in: Geol. Soc. Am. Mem., vol. 194, 171–197, https://doi.org/10.1130/0-8137-1194-0.171, 2001.

Deng, H., McClay, K., and Bilal, A.: 3D structure and evolution of an extensional fault network of the eastern Dampier Sub-basin, North West Shelf of Australia, Journal of Structural Geology, 132, 103972, https://doi.org/10.1016/j.jsg.2019.103972, 2020.

Deng, Q., Ran, Y., Yang, X., Min, W., and Chu, Q.: Map of Active tectonics in China, Seismological Press, Beijing, 2007.

Densmore, A. L., Dawers, N. H., Gupta, S., Allen, P. A., and Gilpin, R.: Landscape evolution at extensional relay zones, Journal of Geophysical Research: Solid Earth, 108, https://doi.org/10.1029/2001JB001741, 2003.

Densmore, A. L., Dawers, N. H., Gupta, S., Guidon, R., and Goldin, T.: Footwall topographic development during continental extension, Journal of Geophysical Research: Earth Surface, 109, https://doi.org/10.1029/2003JF000115, 2004.

Di Giacomo, D., Engdahl, E. R., and Storchak, D. A.: The ISC-GEM Earthquake Catalogue (1904–2014): status after the Extension Project, Earth Syst. Sci. Data, 10, 1877–1899, https://doi.org/10.5194/essd-10-1877-2018, 2018.

DiBiase, R. A., Whipple, K. X., Heimsath, A. M., and Ouimet, W. B.: Landscape form and millennial erosion rates in the San Gabriel Mountains, CA, Earth and Planetary Science Letters, 289, 134–144, https://doi.org/10.1016/j.epsl.2009.10.036, 2010.

Dong, S., Zhang, Y., Zhang, F., Cui, J., Chen, X., Zhang, S., Miao, L., Li, J., Shi, W., Li, Z., Huang, S., and Li, H.: Late Jurassic–Early Cretaceous continental convergence and intracontinental orogenesis in East Asia: A synthesis of the Yanshan Revolution, Journal of Asian Earth Sciences, 114, 750–770, https://doi.org/10.1016/j.jseaes.2015.08.011, 2015.

Dulanya, Z., Gallen, S. F., Kolawole, F., Williams, J. N., Wedmore, L. N. J., Biggs, J., and Fagereng, Å.: Knickpoint morphotectonics of the Middle Shire River basin: Implications for the evolution of rift interaction zones, Basin Research, 34, 1839–1858, https://doi.org/10.1111/bre.12687, 2022.

Dunbar, J. A. and Sawyer, D. S.: Continental rifting at pre-existing lithospheric weaknesses, Nature, 333, 450–452, https://doi.org/10.1038/333450a0, 1988.

Ebinger, C. J., Rosendahl, B. R., and Reynolds, D. J.: Tectonic model of the Malaŵi rift, Africa, Tectonophysics, 141, 215–235, https://doi.org/10.1016/0040-1951(87)90187-9, 1987.

Ebinger, C. J., Reiss, M. C., Bastow, I., and Karanja, M. M.: Shallow sources of upper mantle seismic anisotropy in East Africa, Earth and Planetary Science Letters, 625, 118488, https://doi.org/10.1016/j.epsl.2023.118488, 2024.

Erbello, A., Melnick, D., Zeilinger, G., Bookhagen, B., Pingel, H., and Strecker, M. R.: Geomorphic expression of a tectonically active rift-transfer zone in southern Ethiopia, Geomorphology, 403, 108162, https://doi.org/10.1016/j.geomorph.2022.108162, 2022.

Farangitakis, G. P., Heron, P. J., McCaffrey, K. J. W., van Hunen, J., and Kalnins, L. M.: The impact of oblique inheritance and changes in relative plate motion on the development of rift-transform systems, Earth and Planetary Science Letters, 541, 116277, https://doi.org/10.1016/j.epsl.2020.116277, 2020.

Faulds, J. E. and Varga, R. J.: The role of accommodation zones and transfer zones in the regional segmentation of extended terranes, in: Accommodation zones and transfer zones; the regional segmentation of the Basin and Range Province, vol. 323, edited by: Faulds, J. E. and Stewart, J. H., Geological Society of America, 0, https://doi.org/10.1130/0-8137-2323-X.1, 1998.

Faure, M., Trap, P., Lin, W., Monié, P., and Bruguier, O.: Polyorogenic evolution of the Paleoproterozoic Trans-North China Belt—New insights from the Lüliangshan-Hengshan-Wutaishan and Fuping massifs, Episodes Journal of International Geoscience, 30, 96–107, 2007.

Fazlikhani, H., Fossen, H., Gawthorpe, R. L., Faleide, J. I., and Bell, R. E.: Basement structure and its influence on the structural configuration of the northern North Sea rift, Tectonics, 36, 1151–1177, https://doi.org/10.1002/2017TC004514, 2017.

Fernández-Blanco, D., de Gelder, G., Lacassin, R., and Armijo, R.: Geometry of Flexural Uplift by Continental Rifting in Corinth, Greece, Tectonics, 39, e2019TC005685, https://doi.org/10.1029/2019TC005685, 2020.

Fick, S. E. and Hijmans, R. J.: WorldClim 2: new 1-km spatial resolution climate surfaces for global land areas, International Journal of Climatology, 37, 4302–4315, https://doi.org/10.1002/joc.5086, 2017.

Fisher, J. A., Pazzaglia, F. J., Anastasio, D. J., and Gallen, S. F.: Linear Inversion of Fluvial Topography in the Northern Apennines: Comparison of Base-Level Fall to Crustal Shortening, Tectonics, 41, e2022TC007379, https://doi.org/10.1029/2022TC007379, 2022.

Flint, J.-J.: Stream gradient as a function of order, magnitude, and discharge, Water Resources Research, 10, 969–973, 1974.

Ford, M., Rohais, S., Williams, E. A., Bourlange, S., Jousselin, D., Backert, N., and Malartre, F.: Tectono-sedimentary evolution of the western Corinth rift (Central Greece), Basin Research, 25, 3–25, https://doi.org/10.1111/j.1365-2117.2012.00550.x, 2013.

Fossen, H. and Rotevatn, A.: Fault linkage and relay structures in extensional settings—A review, Earth-Science Reviews, 154, 14–28, https://doi.org/10.1016/j.earscirev.2015.11.014, 2016.

Fraser, A. J. and Gawthorpe, R. L.: Tectono-stratigraphic development and hydrocarbon habitat of the Carboniferous in northern England, Geological Society, London, Special Publications, 55, 49–86, https://doi.org/10.1144/GSL.SP.1990.055.01.03, 1990.

Friedmann, S. J. and Burbank, D. W.: Rift basins and supradetachment basins: intracontinental extensional end-members, Basin Research, 7, 109–127, https://doi.org/10.1111/j.1365-2117.1995.tb00099.x, 1995.

Gallen, S. F. and Fernández-Blanco, D.: A New Data-Driven Bayesian Inversion of Fluvial Topography Clarifies the Tectonic History of the Corinth Rift and Reveals a Channel Steepness Threshold, Journal of Geophysical Research: Earth Surface, 126, e2020JF005651, https://doi.org/10.1029/2020JF005651, 2021.

Gao, M., Zeilinger, G., Xu, X., Tan, X., Wang, Q., and Hao, M.: Active tectonics evaluation from geomorphic indices for the central and the southern Longmenshan range on the Eastern Tibetan Plateau, China, Tectonics, 35, 1812–1826, https://doi.org/10.1002/2015TC004080, 2016.

Gao, S., Davis, P. M., Liu, H., Slack, P. D., Rigor, A. W., Zorin, Y. A., Mordvinova, V. V., Kozhevnikov, V. M., and Logatchev, N. A.: SKS splitting beneath continental rift zones, Journal of Geophysical Research: Solid Earth, 102, 22781–22797, https://doi.org/10.1029/97JB01858, 1997.

Gao, S., Rudnick, R. L., Carlson, R. W., McDonough, W. F., and Liu, Y.-S.: Re–Os evidence for replacement of ancient mantle lithosphere beneath the North China craton, Earth and Planetary Science Letters, 198, 307–322, https://doi.org/10.1016/S0012-821X(02)00489-2, 2002.

Gao, S., Rudnick, R. L., Yuan, H.-L., Liu, X.-M., Liu, Y.-S., Xu, W.-L., Ling, W.-L., Ayers, J., Wang, X.-C., and Wang, Q.-H.: Recycling lower continental crust in the North China craton, Nature, 432, 892–897, https://doi.org/10.1038/nature03162, 2004.

Gardner, T. W.: The History of Part of the Colorado River and Its Tributaries: An Experimental Study, 87–95, 1975.

Gavel, M. M., Amato, J. M., Ricketts, J. W., Kelley, S., Biddle, J. M., and Delfin, R. A.: Thermochronological transect across the Basin and Range/Rio Grande rift transition: Contrasting cooling histories in contiguous extensional provinces, Geosphere, 17, 1807–1839, https://doi.org/10.1130/GES02381.1, 2021.

Gawthorpe, R. L. and Hurst, J. M.: Transfer zones in extensional basins: their structural style and influence on drainage development and stratigraphy, Journal of the Geological Society, 150, 1137–1152, https://doi.org/10.1144/gsjgs.150.6.1137, 1993.

Gawthorpe, R. L. and Leeder, M. R.: Tectono-sedimentary evolution of active extensional basins, Basin Research, 12, 195–218, https://doi.org/10.1111/j.1365-2117.2000.00121.x, 2000a.

Gawthorpe, R. L. and Leeder, M. R.: Tectono-sedimentary evolution of active extensional basins, Basin Research, 12, 195–218, https://doi.org/10.1111/j.1365-2117.2000.00121.x, 2000b.

Geurts, A. H., Whittaker, A. C., Gawthorpe, R. L., and Cowie, P. A.: Transient landscape and stratigraphic responses to drainage integration in the actively extending central Italian Apennines, Geomorphology, 353, 107013, https://doi.org/10.1016/j.geomorph.2019.107013, 2020.

Goldsworthy, M. and Jackson, J.: Active normal fault evolution in Greece revealed by geomorphology and drainage patterns, Journal of the Geological Society, 157, 967–981, https://doi.org/10.1144/jgs.157.5.967, 2000.

Griffin, B., Andi, Z., O'Reilly, S., and Ryan, C.: Phanerozoic evolution of the lithosphere beneath the Sino-Korean craton: Conference on Mantle Dynamics and Plate Interactions in East Asia, Mantle dynamics and plate interactions in east Asia, 107–126, 1998.

Groves, K., Saville, C., Hurst, M. D., Jones, S. J., Song, S., and Allen, M. B.: Geomorphic expressions of collisional tectonics in the Qilian Shan, north eastern Tibetan Plateau, Tectonophysics, 788, 228503, https://doi.org/10.1016/j.tecto.2020.228503, 2020.

Hack, J. T.: Studies of longitudinal stream profiles in Virginia and Maryland, US Government Printing Office, 1957.

Hamdouni, R., Irigaray, C., Castillo, T., Chacón, J., and Keller, E.: Assessment of relative active tectonics, southwest border of the Sierra Nevada (southern Spain), Geomorphology, 150–173, https://doi.org/10.1016/j.geomorph.2007.08.004, 2008.

Harden, D. R.: Controlling factors in the distribution and development of incised meanders in the central Colorado Plateau, GSA Bulletin, 102, 233–242, https://doi.org/10.1130/0016-7606(1990)102<0233:CFITDA>2.3.CO;2, 1990.

Harkins, N. W., Anastasio, D. J., and Pazzaglia, F. J.: Tectonic geomorphology of the Red Rock fault, insights into segmentation and landscape evolution of a developing range front normal fault, Journal of Structural Geology, 27, 1925–1939, https://doi.org/10.1016/j.jsg.2005.07.005, 2005.

He, J., Liu, M., and Li, Y.: Is the Shanxi rift of northern China extending?, Geophysical research letters, 30, 2003.

Heilman, E., Kolawole, F., Atekwana, E. A., and Mayle, M.: Controls of Basement Fabric on the Linkage of Rift Segments, Tectonics, 38, 1337–1366, https://doi.org/10.1029/2018TC005362, 2019.

Henstra, G. A., Rotevatn, A., Gawthorpe, R. L., and Ravnås, R.: Evolution of a major segmented normal fault during multiphase rifting: The origin of plan-view zigzag geometry, Journal of Structural Geology, 74, 45–63, https://doi.org/10.1016/j.jsg.2015.02.005, 2015.

Henza, A. A., Withjack, M. O., and Schlische, R. W.: How do the properties of a pre-existing normal-fault population influence fault development during a subsequent phase of extension?, Journal of Structural Geology, 33, 1312–1324, https://doi.org/10.1016/j.jsg.2011.06.010, 2011.

Heron, P. J., Peace, A. L., McCaffrey, K. J. W., Welford, J. K., Wilson, R., van Hunen, J., and Pysklywec, R. N.: Segmentation of Rifts Through Structural Inheritance: Creation of the Davis Strait, Tectonics, 38, 2411–2430, https://doi.org/10.1029/2019TC005578, 2019.

Hodge, M., Fagereng, Å., Biggs, J., and Mdala, H.: Controls on early-rift geometry: New perspectives from the Bilila-Mtakataka Fault, Malawi, Geophysical Research Letters, 45, 3896–3905, 2018a.

Hodge, M., Fagereng, Å., and Biggs, J.: The Role of Coseismic Coulomb Stress Changes in Shaping the Hard Link Between Normal Fault Segments, Journal of Geophysical Research: Solid Earth, 123, 797–814, https://doi.org/10.1002/2017JB014927, 2018b.

Holdsworth, R. E., Stewart, M., Imber, J., and Strachan, R. A.: The structure and rheological evolution of reactivated continental fault zones: a review and case study, Geological Society, London, Special Publications, 184, 115–137, https://doi.org/10.1144/GSL.SP.2001.184.01.07, 2001.

Howell, L., Egan, S., Leslie, G., Clarke, S., Mitten, A., and Pringle, J.: The influence of low-density granite bodies on extensional basins, Geology Today, 36, 22–26, https://doi.org/10.1111/gto.12297, 2020.

Hu, X., Li, Y., and Yang, J.: Quaternary paleolake development in the Fen River basin, North China, Geomorphology, 65, 1–13, https://doi.org/10.1016/j.geomorph.2004.06.008, 2005.

Hurtrez, J.-E., Sol, C., and Lucazeau, F.: Effect of drainage area on hypsometry from an analysis of small-scale drainage basins in the Siwalik Hills (Central Nepal), Earth Surface Processes and Landforms, 24, 799–808, https://doi.org/10.1002/(SICI)1096-9837(199908)24:9<799::AID-ESP12>3.0.CO;2-4, 1999a.

Hurtrez, J.-E., Sol, C., and Lucazeau, F.: Effect of drainage area on hypsometry from an analysis of small-scale drainage basins in the Siwalik Hills (Central Nepal), Earth Surface Processes and Landforms, 24, 799–808, https://doi.org/10.1002/(SICI)1096-9837(199908)24:9<799::AID-ESP12>3.0.CO;2-4, 1999b.

Jackson, J. and Leeder, M.: Drainage systems and the development of normal faults: an example from Pleasant Valley, Nevada, Journal of Structural Geology, 16, 1041–1059, https://doi.org/10.1016/0191-8141(94)90051-5, 1994.

Kapp, P., Pullen, A., Pelletier, J. D., Russell, J., Goodman, P., and Cai, F.: From dust to dust: Quaternary wind erosion of the Mu Us Desert and Loess Plateau, China, Geology, 43, 835–838, https://doi.org/10.1130/G36724.1, 2015.

Kattenhorn, S. A., Aydin, A., and Pollard, D. D.: Joints at high angles to normal fault strike: an explanation using 3-D numerical models of fault-perturbed stress fields, Journal of Structural Geology, 22, 1–23, https://doi.org/10.1016/S0191-8141(99)00130-3, 2000.

Kendall, J.-M., Pilidou, S., Keir, D., Bastow, I. D., Stuart, G. W., and Ayele, A.: Mantle upwellings, melt migration and the rifting of Africa: insights from seismic anisotropy, Geological Society, London, Special Publications, 259, 55–72, https://doi.org/10.1144/GSL.SP.2006.259.01.06, 2006.

Kinabo, B. D., Hogan, J. P., Atekwana, E. A., Abdelsalam, M. G., and Modisi, M. P.: Fault growth and propagation during incipient continental rifting: Insights from a combined aeromagnetic and Shuttle Radar Topography Mission digital elevation model investigation of the Okavango Rift Zone, northwest Botswana, Tectonics, 27, https://doi.org/10.1029/2007TC002154, 2008.

Kirby, E. and Whipple, K. X.: Expression of active tectonics in erosional landscapes, Journal of Structural Geology, 44, 54–75, https://doi.org/10.1016/j.jsg.2012.07.009, 2012.

Koehn, D., Aanyu, K., Haines, S., and Sachau, T.: Rift nucleation, rift propagation and the creation of basement micro-plates within active rifts, Tectonophysics, 458, 105–116, https://doi.org/10.1016/j.tecto.2007.10.003, 2008.

Kolawole, F., Atekwana, E. A., Laó-Dávila, D. A., Abdelsalam, M. G., Chindandali, P. R., Salima, J., and Kalindekafe, L.: Active deformation of Malawi rift's north basin Hinge zone modulated by reactivation of preexisting Precambrian Shear zone fabric, Tectonics, 37, 683–704, 2018.

Kolawole, F., Firkins, M. C., Al Wahaibi, T. S., Atekwana, E. A., and Soreghan, M. J.: Rift interaction zones and the stages of rift linkage in active segmented continental rift systems, Basin Research, 33, 2984–3020, 2021a.

Kolawole, F., Phillips, T. B., Atekwana, E. A., and Jackson, C. A.-L.: Structural Inheritance Controls Strain Distribution During Early Continental Rifting, Rukwa Rift, Front. Earth Sci., 9, https://doi.org/10.3389/feart.2021.707869, 2021b.

Kolawole, F., Vick, T., Atekwana, E. A., Laó-Dávila, D. A., Costa, A. G., and Carpenter, B. M.: Strain localization and migration during the pulsed lateral propagation of the Shire Rift Zone, East Africa, Tectonophysics, 839, 229499, https://doi.org/10.1016/j.tecto.2022.229499, 2022.

Kolawole, F., Xue, L., and Dulanya, Z.: Rapid Versus Delayed Linkage and Coalescence of Propagating Rift Tips, https://doi.org/10.22541/essoar.168167202.29986035/v2, 4 March 2024.

Krabbendam, M. and Barr, T. D.: Proterozoic orogens and the break-up of Gondwana: why did some orogens not rift?, Journal of African Earth Sciences, 31, 35–49, https://doi.org/10.1016/S0899-5362(00)00071-3, 2000a.

Krabbendam, M. and Barr, T. D.: Proterozoic orogens and the break-up of Gondwana: why did some orogens not rift?, Journal of African Earth Sciences, 31, 35–49, https://doi.org/10.1016/S0899-5362(00)00071-3, 2000b.

Kusky, T., Li, J., and Santosh, M.: The Paleoproterozoic North Hebei Orogen: North China craton's collisional suture with the Columbia supercontinent, Gondwana Research, 12, 4–28, https://doi.org/10.1016/j.gr.2006.11.012, 2007.

Kusky, T. M. and Li, J.: Paleoproterozoic tectonic evolution of the North China Craton, Journal of Asian Earth Sciences, 22, 383–397, https://doi.org/10.1016/S1367-9120(03)00071-3, 2003.

Lambiase, J. J. and Bosworth, W.: Structural controls on sedimentation in continental rifts, Geological Society, London, Special Publications, 80, 117–144, https://doi.org/10.1144/GSL.SP.1995.080.01.06, 1995.

Leeder, M. R. and Jackson, J. A.: The interaction between normal faulting and drainage in active extensional basins, with examples from the western United States and central Greece, Basin Research, 5, 79–102, https://doi.org/10.1111/j.1365-2117.1993.tb00059.x, 1993.

Leonard, M.: Earthquake Fault Scaling: Self-Consistent Relating of Rupture Length, Width, Average Displacement, and Moment Release, Bulletin of the Seismological Society of America, 100, 1971–1988, https://doi.org/10.1785/0120090189, 2010.

Lezzar, K. E., Tiercelin, J.-J., Le Turdu, C., Cohen, Andrew. S., Reynolds, D. J., Le Gall, B., and Scholz, C. A.: Control of Normal Fault Interaction on the Distribution of Major Neogene Sedimentary Depocenters, Lake Tanganyika, East African Rift, AAPG Bulletin, 86, 1027–1059, https://doi.org/10.1306/61EEDC1A-173E-11D7-8645000102C1865D, 2002.

Li, S., Zhao, G., Wilde, S. A., Zhang, J., Sun, M., Zhang, G., and Dai, L.: Deformation history of the Hengshan–Wutai–Fuping Complexes: Implications for the evolution of the Trans-North China Orogen, Gondwana Research, 18, 611–631, https://doi.org/10.1016/j.gr.2010.03.003, 2010.

Li, Y., Yang, J., Xia, Z., and Mo, D.: Tectonic geomorphology in the Shanxi Graben System, northern China, Geomorphology, 23, 77–89, https://doi.org/10.1016/S0169-555X(97)00092-5, 1998.

Lifton, N. A. and Chase, C. G.: Tectonic, climatic and lithologic influences on landscape fractal dimension and hypsometry: implications for landscape evolution in the San Gabriel Mountains, California, Geomorphology, 5, 77–114, https://doi.org/10.1016/0169-555X(92)90059-W, 1992.

Maerten, L.: Variation in slip on intersecting normal faults: Implications for paleostress inversion, Journal of Geophysical Research: Solid Earth, 105, 25553–25565, https://doi.org/10.1029/2000JB900264, 2000.

Makrari, S., Sharma, G., Taloor, A. K., Singh, M. S., Sarma, K. K., and Aggarwal, S. P.: Assessment of the geomorphic indices in relation to tectonics along selected sectors of Borpani River Basin, Assam using Cartosat DEM data, Geosystems and Geoenvironment, 1, 100068, https://doi.org/10.1016/j.geogeo.2022.100068, 2022.

Masek, J. G., Isacks, B. L., Gubbels, T. L., and Fielding, E. J.: Erosion and tectonics at the margins of continental plateaus, Journal of Geophysical Research: Solid Earth, 99, 13941–13956, https://doi.org/10.1029/94JB00461, 1994.

McCaffrey, K. J. W.: Controls on reactivation of a major fault zone: the Fair Head–Clew Bay line in Ireland, Journal of the Geological Society, 154, 129–133, https://doi.org/10.1144/gsjgs.154.1.0129, 1997.

Menzies, M., Xu, Y., Zhang, H., and Fan, W.: Integration of geology, geophysics and geochemistry: A key to understanding the North China Craton, Lithos, 96, 1–21, https://doi.org/10.1016/j.lithos.2006.09.008, 2007.

Menzies, M. A. and Xu, Y.: Geodynamics of the North China Craton, in: Mantle Dynamics and Plate Interactions in East Asia, American Geophysical Union (AGU), 155–165, https://doi.org/10.1029/GD027p0155, 1998.

Menzies, M. A., Fan, W., and Zhang, M.: Palaeozoic and Cenozoic lithoprobes and the loss of >120 km of Archaean lithosphere, Sino-Korean craton, China, Geological Society, London, Special Publications, 76, 71–81, https://doi.org/10.1144/GSL.SP.1993.076.01.04, 1993.

Middleton, T. A., Elliott, J. R., Rhodes, E. J., Sherlock, S., Walker, R. T., Wang, W., Yu, J., and Zhou, Y.: Extension rates across the northern Shanxi Grabens, China, from Quaternary geology, seismicity and geodesy, Geophysical Journal International, 209, 535–558, 2017.

Molnar, N., Cruden, A., and Betts, P.: The role of inherited crustal and lithospheric architecture during the evolution of the Red Sea: Insights from three dimensional analogue experiments, Earth and Planetary Science Letters, 544, 116377, https://doi.org/10.1016/j.epsl.2020.116377, 2020.

Moore, J. M. and Davidson, A.: Rift structure in southern Ethiopia, Tectonophysics, 46, 159–173, https://doi.org/10.1016/0040-1951(78)90111-7, 1978.

Morley, C. K.: Variable extension in Lake Tanganyika, Tectonics, 7, 785–801, https://doi.org/10.1029/TC007i004p00785, 1988.

Morley, C. K.: Stress re-orientation along zones of weak fabrics in rifts: An explanation for pure extension in 'oblique' rift segments?, Earth and Planetary Science Letters, 297, 667–673, https://doi.org/10.1016/j.epsl.2010.07.022, 2010.

Morley, C. K., Nelson, R. A., Patton, T. L., and Munn, S. G.: Transfer Zones in the East African Rift System and Their Relevance to Hydrocarbon Exploration in Rifts1, AAPG Bulletin, 74, 1234–1253, https://doi.org/10.1306/0C9B2475-1710-11D7-8645000102C1865D, 1990.

Morley, C. K., Haranya, C., Phoosongsee, W., Pongwapee, S., Kornsawan, A., and Wonganan, N.: Activation of rift oblique and rift parallel pre-existing fabrics during extension and their effect on deformation style: examples from the rifts of Thailand, Journal of Structural Geology, 26, 1803–1829, https://doi.org/10.1016/j.jsg.2004.02.014, 2004.

Mulaya, E., Gluyas, J., McCaffrey, K., Phillips, T., and Ballentine, C.: Structural geometry and evolution of the Rukwa Rift Basin, Tanzania: Implications for helium potential, Basin Research, 34, 938–960, https://doi.org/10.1111/bre.12646, 2022.

Musila, M., Ebinger, C. J., Bastow, I. D., Sullivan, G., Oliva, S. J., Knappe, E., Perry, M., Kounoudis, R., Ogden, C. S., Bendick, R., Mwangi, S., Mariita, N., Kianji, G., Kraus, E., and Illsley-Kemp, F.: Active Deformation Constraints on the Nubia-Somalia Plate Boundary Through Heterogenous Lithosphere of the Turkana Depression, Geochemistry, Geophysics, Geosystems, 24, e2023GC010982, https://doi.org/10.1029/2023GC010982, 2023.

Nelson, R. A., Patton, T. L., and Morley, C. K.: Rift-Segment Interaction and Its Relation to Hydrocarbon Exploration in Continental Rift Systems (1), AAPG Bulletin, 76, 1153–1169, 1992.

Obaid, A. K. and Allen, M. B.: Landscape expressions of tectonics in the Zagros fold-and-thrust belt, Tectonophysics, 766, 20–30, https://doi.org/10.1016/j.tecto.2019.05.024, 2019.

Osagiede, E. E., Rotevatn, A., Gawthorpe, R., Kristensen, T. B., Jackson, C. A.-L., and Marsh, N.: Pre-existing intra-basement shear zones influence growth and geometry of non-colinear normal faults, western Utsira High–Heimdal Terrace, North Sea, Journal of Structural Geology, 130, 103908, https://doi.org/10.1016/j.jsg.2019.103908, 2020.

Pavlides, S. B., Zouros, N. C., Zhongjing, F., Shaoping, C., Tranos, M. D., and Chatzipetros, A. A.: Geometry, kinematics and morphotectonics of the Yanqing–Huailai active faults (northern China), Tectonophysics, 308, 99–118, https://doi.org/10.1016/S0040-1951(99)00074-8, 1999.

Peace, A., McCaffrey, K., Imber, J., Hunen, J. van, Hobbs, R., and Wilson, R.: The role of pre-existing structures during rifting, continental breakup and transform system development, offshore West Greenland, Basin Research, 30, 373–394, https://doi.org/10.1111/bre.12257, 2018.

Pérez-Peña, J. V., Azañón, J. M., Booth-Rea, G., Azor, A., and Delgado, J.: Differentiating geology and tectonics using a spatial autocorrelation technique for the hypsometric integral, Journal of Geophysical Research: Earth Surface, 114, https://doi.org/10.1029/2008JF001092, 2009.

Perron, J. T. and Royden, L.: An integral approach to bedrock river profile analysis, Earth Surface Processes and Landforms, 38, 570–576, https://doi.org/10.1002/esp.3302, 2013.

Petit, C., Deverchere, J., Houdry, F., Sankov, V. A., Melnikova, V. I., and Delvaux, D.: Present-day stress field changes along the Baikal rift and tectonic implications, Tectonics, 15, 1171–1191, 1996.

Philippon, M., Willingshofer, E., Sokoutis, D., Corti, G., Sani, F., Bonini, M., and Cloetingh, S.: Slip re-orientation in oblique rifts, Geology, 43, 147–150, 2015.

Phillips, T. B. and McCaffrey, K. J. W.: Terrane Boundary Reactivation, Barriers to Lateral Fault Propagation and Reactivated Fabrics: Rifting Across the Median Batholith Zone, Great South Basin, New Zealand, Tectonics, 38, 4027–4053, https://doi.org/10.1029/2019TC005772, 2019.

Phillips, T. B., Jackson, C. A., Bell, R. E., Duffy, O. B., and Fossen, H.: Reactivation of intrabasement structures during rifting: A case study from offshore southern Norway, Journal of Structural Geology, 91, 54–73, 2016.

Phillips, T. B., Naliboff, J. B., McCaffrey, K. J. W., Pan, S., van Hunen, J., and Froemchen, M.: The influence of crustal strength on rift geometry and development – insights from 3D numerical modelling, Solid Earth, 14, 369–388, https://doi.org/10.5194/se-14-369-2023, 2023.

Qi, J. and Yang, Q.: Cenozoic structural deformation and dynamic processes of the Bohai Bay basin province, China, Marine and Petroleum Geology, 27, 757–771, https://doi.org/10.1016/j.marpetgeo.2009.08.012, 2010.

Ramos, G. V., Vasconcelos, D. L., Marques, F. O., de Castro, D. L., Nogueira, F. C. C., Bezerra, F. H. R., Perez, Y. A. R., Souza, J. A. B., and Medeiros, V. C.: Relations between inherited basement fabric and fault nucleation in a continental setting: The Rio do Peixe Basin, NE Brazil, Marine and Petroleum Geology, 139, 105635, https://doi.org/10.1016/j.marpetgeo.2022.105635, 2022.

Reeve, M. T., Bell, R. E., Duffy, O. B., Jackson, C. A.-L., and Sansom, E.: The growth of non-colinear normal fault systems; What can we learn from 3D seismic reflection data?, Journal of Structural Geology, 70, 141–155, 2015.

Ring, U.: The influence of preexisting structure on the evolution of the Cenozoic Malawi rift (East African rift system), Tectonics, 13, 313–326, https://doi.org/10.1029/93TC03188, 1994.

Rosendahl, B. R.: Architecture of Continental Rifts with Special Reference to East Africa, Annual Review of Earth and Planetary Sciences, 15, 445–503, https://doi.org/10.1146/annurev.ea.15.050187.002305, 1987.

Rotevatn, A., Kristensen, T. B., Ksienzyk, A. K., Wemmer, K., Henstra, G. A., Midtkandal, I., Grundvåg, S.-A., and Andresen, A.: Structural Inheritance and Rapid Rift-Length Establishment in a Multiphase Rift: The East Greenland Rift System and its Caledonian Orogenic Ancestry, Tectonics, 37, 1858–1875, https://doi.org/10.1029/2018TC005018, 2018.

Sachau, T., Koehn, D., Stamps, D. S., and Lindenfeld, M.: Fault kinematics and stress fields in the Rwenzori Mountains, Uganda, Int J Earth Sci (Geol Rundsch), 105, 1729–1740, https://doi.org/10.1007/s00531-015-1162-6, 2016.

Samsu, A., Cruden, A. R., Micklethwaite, S., Grose, L., and Vollgger, S. A.: Scale matters: The influence of structural inheritance on fracture patterns, Journal of Structural Geology, 130, 103896, https://doi.org/10.1016/j.jsg.2019.103896, 2020.

Samsu, A., Micklethwaite, S., Williams, J. N., Fagereng, Å., and Cruden, A. R.: Structural inheritance in amagmatic rift basins: Manifestations and mechanisms for how pre-existing structures influence rift-related faults, Earth-Science Reviews, 246, 104568, https://doi.org/10.1016/j.earscirev.2023.104568, 2023.

Santosh, M.: Assembling North China Craton within the Columbia supercontinent: The role of double-sided subduction, Precambrian Research, 178, 149–167, https://doi.org/10.1016/j.precamres.2010.02.003, 2010.

Schiffer, C., Doré, A. G., Foulger, G. R., Franke, D., Geoffroy, L., Gernigon, L., Holdsworth, B., Kusznir, N., Lundin, E., McCaffrey, K., Peace, A. L., Petersen, K. D., Phillips, T. B., Stephenson, R., Stoker, M. S., and Welford, J. K.: Structural inheritance in the North Atlantic, Earth-Science Reviews, 206, 102975, https://doi.org/10.1016/j.earscirev.2019.102975, 2020.

Schmidt, K. M. and Montgomery, D. R.: Limits to Relief, Science, 270, 617–620, https://doi.org/10.1126/science.270.5236.617, 1995.

Scholz, C. A.: Deltas of the Lake Malawi Rift, East Africa: Seismic Expression and Exploration Implications 1, AAPG Bulletin, 79, 1679–1697, https://doi.org/10.1306/7834DE54-1721-11D7-8645000102C1865D, 1995.

Scholz, C. H.: Scaling laws for large earthquakes: Consequences for physical models, Bulletin of the Seismological Society of America, 72, 1–14, https://doi.org/10.1785/BSSA0720010001, 1982.

Schumacher, M. E.: Upper Rhine Graben: Role of preexisting structures during rift evolution, Tectonics, 21, 6-1-6–17, https://doi.org/10.1029/2001TC900022, 2002.

Schwanghart, W. and Scherler, D.: Short Communication: TopoToolbox 2 – MATLAB-based software for topographic analysis and modeling in Earth surface sciences, Earth Surface Dynamics, 2, 1–7, https://doi.org/10.5194/esurf-2-1-2014, 2014.

Şengör, A. M. C., Lom, N., and Sağdıç, N. G.: Tectonic inheritance, structure reactivation and lithospheric strength: the relevance of geological history, Geological Society, London, Special Publications, 470, 105–136, https://doi.org/10.1144/SP470.8, 2019.

Shanxi Bureau of Geology and Mineral Resources (SBGMR): Regional Geology of Shanxi Province, Geological Publishing House, Beijing, China, 1989.

Shen, Z.-K., Zhao, C., Yin, A., Li, Y., Jackson, D. D., Fang, P., and Dong, D.: Contemporary crustal deformation in east Asia constrained by Global Positioning System measurements, Journal of Geophysical Research: Solid Earth, 105, 5721–5734, https://doi.org/10.1029/1999JB900391, 2000.

Shi, W., Dong, S., Liu, Y., Hu, J., Chen, X., and Chen, P.: Cenozoic tectonic evolution of the South Ningxia region, northeastern Tibetan Plateau inferred from new structural investigations and fault kinematic analyses, Tectonophysics, 649, 139–164, https://doi.org/10.1016/j.tecto.2015.02.024, 2015a.

Shi, W., Cen, M., Chen, L., Wang, Y., Chen, X., Li, J., and Chen, P.: Evolution of the late Cenozoic tectonic stress regime in the Shanxi Rift, central North China Plate inferred from new fault kinematic analysis, Journal of Asian Earth Sciences, 114, 54–72, https://doi.org/10.1016/j.jseaes.2015.04.044, 2015b.

Shi, W., Dong, S., and Hu, J.: Neotectonics around the Ordos Block, North China: A review and new insights, Earth-Science Reviews, 200, 102969, 2020.

Snyder, N. P., Whipple, K. X., Tucker, G. E., and Merritts, D. J.: Landscape response to tectonic forcing: Digital elevation model analysis of stream profiles in the Mendocino triple junction region, northern California, Geological Society of America Bulletin, 112, 1250–1263, 2000.

Storchak, D. A., Di Giacomo, D., Bondar, I., Engdahl, E. R., Harris, J., Lee, W. H. K., Villasenor, A., and Bormann, P.: Public Release of the ISC-GEM Global Instrumental Earthquake Catalogue (1900-2009), Seismological Research Letters, 84, 810–815, https://doi.org/10.1785/0220130034, 2013.

Storchak, D. A., Di Giacomo, D., Engdahl, E. R., Harris, J., Bondár, I., Lee, W. H., Bormann, P., and Villaseñor, A.: The ISC-GEM global instrumental earthquake catalogue (1900–2009): introduction, Physics of the Earth and Planetary Interiors, 239, 48–63, 2015.

Strahler, A. N.: Hypsometirc (area-altitude) Analysis of erosional topography, GSA Bulletin, 63, 1117–1142, https://doi.org/10.1130/0016-7606(1952)63[1117:HAAOET]2.0.CO;2, 1952.

Strahler, A. N.: Quantitative analysis of watershed geomorphology, Eos, Transactions American Geophysical Union, 38, 913–920, https://doi.org/10.1029/TR038i006p00913, 1957.

Su, P., He, H., Tan, X., Liu, Y., Shi, F., and Kirby, E.: Initiation and evolution of the Shanxi Rift System in North China: Evidence from low-temperature thermochronology in a plate reconstruction framework, Tectonics, 40, e2020TC006298, 2021.

Su, P., He, H., Liu, Y., Shi, F., Granger, D. E., Kirby, E., Luo, L., Han, F., and Lu, R.: Quantifying the Structure and Extension Rate of the Linfen Basin, Shanxi Rift System Since the Latest Miocene: Implications for Continental Magma-Poor Rifting, Tectonics, 42, e2023TC007885, https://doi.org/10.1029/2023TC007885, 2023.

Tang Y.-C., Fen Y.-G., Chen Zhongshun J., Zhou S.-Y., Ning J.-Y., Wei S.-Q., Li P., Chun-Quan Y., Fan W.-Y., and Wang H.-Y.: Receiver function analysis at Shanxi Rift, Chinese Journal of Geophysics, 53, 2102–2109, https://doi.org/10.3969/j.issn.0001-5733.2010.09.010, 2010.

Taylor, S. K., Bull, J. M., Lamarche, G., and Barnes, P. M.: Normal fault growth and linkage in the Whakatane Graben, New Zealand, during the last 1.3 Myr, Journal of Geophysical Research: Solid Earth, 109, https://doi.org/10.1029/2003JB002412, 2004.

Tepp, G., Ebinger, C. J., Zal, H., Gallacher, R., Accardo, N., Shillington, D. J., Gaherty, J., Keir, D., Nyblade, A. A., Mbogoni, G. J., Chindandali, P. R. N., Ferdinand-Wambura, R., Mulibo, G. D., and Kamihanda, G.: Seismic Anisotropy of the Upper Mantle Below the Western Rift, East Africa, Journal of Geophysical Research: Solid Earth, 123, 5644–5660, https://doi.org/10.1029/2017JB015409, 2018.

Tommasi, A. and Vauchez, A.: Continental rifting parallel to ancient collisional belts: an effect of the mechanical anisotropy of the lithospheric mantle, Earth and Planetary Science Letters, 185, 199–210, https://doi.org/10.1016/S0012-821X(00)00350-2, 2001.

Trap, P., Faure, M., Lin, W., and Monié, P.: Late Paleoproterozoic (1900–1800Ma) nappe stacking and polyphase deformation in the Hengshan–Wutaishan area: Implications for the understanding of the Trans-North-China Belt, North China Craton, Precambrian Research, 156, 85–106, https://doi.org/10.1016/j.precamres.2007.03.001, 2007.

Trap, P., Faure, M., Lin, W., Bruguier, O., and Monié, P.: Contrasted tectonic styles for the Paleoproterozoic evolution of the North China Craton. Evidence for a ∼2.1Ga thermal and tectonic event in the Fuping Massif, Journal of Structural Geology, 30, 1109–1125, https://doi.org/10.1016/j.jsg.2008.05.001, 2008.

Trap, P., Faure, M., Lin, W., and Meffre, S.: The Lüliang Massif: a key area for the understanding of the Palaeoproterozoic Trans-North China Belt, North China Craton, Geological Society, London, Special Publications, 323, 99–125, 2009a.

Trap, P., Faure, M., Lin, W., Monié, P., Meffre, S., and Melleton, J.: The Zanhuang Massif, the second and eastern suture zone of the Paleoproterozoic Trans-North China Orogen, Precambrian Research, 172, 80–98, 2009b.

Trap, P., Faure, M., Lin, W., Le Breton, N., and Monié, P.: Paleoproterozoic tectonic evolution of the Trans-North China Orogen: Toward a comprehensive model, Precambrian Research, 222–223, 191–211, https://doi.org/10.1016/j.precamres.2011.09.008, 2012.

Vasconcelos, D. L., Bezerra, F. H. R., Medeiros, W. E., de Castro, D. L., Clausen, O. R., Vital, H., and Oliveira, R. G.: Basement fabric controls rift nucleation and postrift basin inversion in the continental margin of NE Brazil, Tectonophysics, 751, 23–40, https://doi.org/10.1016/j.tecto.2018.12.019, 2019.

Vauchez, A., Barruol, G., and Tommasi, A.: Why do continents break-up parallel to ancient orogenic belts?, Terra Nova, 9, 62–66, https://doi.org/10.1111/j.1365-3121.1997.tb00003.x, 1997.

Versfelt, J. and Rosendahl, B. R.: Relationships between pre-rift structure and rift architecture in Lakes Tanganyika and Malawi, East Africa, Nature, 337, 354–357, https://doi.org/10.1038/337354a0, 1989.

Vetel, W. and Le Gall, B.: Dynamics of prolonged continental extension in magmatic rifts: the Turkana Rift case study (North Kenya), Geological Society, London, Special Publications, 259, 209–233, https://doi.org/10.1144/GSL.SP.2006.259.01.17, 2006.

Walcott, R. C. and Summerfield, M. A.: Scale dependence of hypsometric integrals: An analysis of southeast African basins, Geomorphology, 96, 174–186, https://doi.org/10.1016/j.geomorph.2007.08.001, 2008.

Wedmore, L. N. J., Williams, J. N., Biggs, J., Fagereng, Å., Mphepo, F., Dulanya, Z., Willoughby, J., Mdala, H., and Adams, B. A.: Structural inheritance and border fault reactivation during active early-stage rifting along the Thyolo fault, Malawi, Journal of Structural Geology, 139, 104097, https://doi.org/10.1016/j.jsg.2020.104097, 2020.

Wedmore, L. N. J., Turner, T., Biggs, J., Williams, J. N., Sichingabula, H. M., Kabumbu, C., and Banda, K.: The Luangwa Rift Active Fault Database and fault reactivation along the southwestern branch of the East African Rift, Solid Earth, 13, 1731–1753, https://doi.org/10.5194/se-13-1731-2022, 2022.

Wheeler, W. H. and Karson, J. A.: Structure and kinematics of the Livingstone Mountains border fault zone, Nyasa (Malawi) Rift, southwestern Tanzania, Journal of African Earth Sciences (and the Middle East), 8, 393–413, https://doi.org/10.1016/S0899-5362(89)80034-X, 1989.

Whipple, K. X.: Bedrock rivers and the geomorphology of active orogens, Annu. Rev. Earth Planet. Sci., 32, 151–185, https://doi.org/10.1146/annurev.earth.32.101802.120356, 2004.

White, R. S., Hardman, R. F. P., Watts, A. B., Whitmarsh, R. B., and Brun, J. –P.: Narrow rifts versus wide rifts: inferences for the mechanics of rifting from laboratory experiments, Philosophical Transactions of the Royal Society of

London. Series A: Mathematical, Physical and Engineering Sciences, 357, 695–712, https://doi.org/10.1098/rsta.1999.0349, 1999.

Whittaker, A. C.: How do landscapes record tectonics and climate?, Lithosphere, 4, 160–164, 2012.

Whittaker, A. C. and Walker, A. S.: Geomorphic constraints on fault throw rates and linkage times: Examples from the Northern Gulf of Evia, Greece, Journal of Geophysical Research: Earth Surface, 120, 137–158, https://doi.org/10.1002/2014JF003318, 2015.

Whittaker, A. C., Attal, M., Cowie, P. A., Tucker, G. E., and Roberts, G.: Decoding temporal and spatial patterns of fault uplift using transient river long profiles, Geomorphology, 100, 506–526, https://doi.org/10.1016/j.geomorph.2008.01.018, 2008.

Williams, J. N., Fagereng, Å., Wedmore, L. N., Biggs, J., Mphepo, F., Dulanya, Z., Mdala, H., and Blenkinsop, T.: How do variably striking faults reactivate during rifting? Insights from southern Malawi, Geochemistry, Geophysics, Geosystems, 20, 3588–3607, 2019.

Wilson, J. T.: Did the Atlantic Close and then Re-Open?, Nature, 211, 676–681, https://doi.org/10.1038/211676a0, 1966.

Wilson, R. W., Holdsworth, R. E., Wild, L. E., McCaffrey, K. J. W., England, R. W., Imber, J., and Strachan, R. A.: Basement-influenced rifting and basin development: a reappraisal of post-Caledonian faulting patterns from the North Coast Transfer Zone, Scotland, Geological Society, London, Special Publications, 335, 795–826, https://doi.org/10.1144/SP335.32, 2010.

Wobus, C., Whipple, K. X., Kirby, E., Snyder, N., Johnson, J., Spyropolou, K., Crosby, B., and Sheehan, D.: Tectonics from topography: Procedures, promise, and pitfalls, in: Tectonics, Climate, and Landscape Evolution, vol. 398, edited by: Willett, S. D., Hovius, N., Brandon, M. T., and Fisher, D. M., Geological Society of America, 0, https://doi.org/10.1130/2006.2398(04), 2006.

Wong, W. H.: Crustal Movements and Igneous Activities in Eastern China Since Mesozoic Time.1, Bulletin of the Geological Society of China, 6, 9–37, https://doi.org/10.1111/j.1755-6724.1927.mp6001002.x, 1927.

Xu, X. and Ma, X.: Geodynamics of the Shanxi rift system, China, Tectonophysics, 208, 325–340, 1992.

Xu, X., Ma, X., and Deng, Q.: Neotectonic activity along the Shanxi rift system, China, Tectonophysics, 219, 305–325, 1993.

Xu, Y., He, H., Deng, Q., Allen, M. B., Sun, H., and Bi, L.: The CE 1303 Hongdong Earthquake and the Huoshan Piedmont Fault, Shanxi Graben: Implications for Magnitude Limits of Normal Fault Earthquakes, J. Geophys. Res. Solid Earth, 123, 3098–3121, https://doi.org/10.1002/2017JB014928, 2018.

Yin, A.: Cenozoic tectonic evolution of Asia: A preliminary synthesis, Tectonophysics, 488, 293–325, https://doi.org/10.1016/j.tecto.2009.06.002, 2010.

Zhai, M., Li, T.-S., Peng, P., Hu, B., Liu, F., and Zhang, Y.: Precambrian key tectonic events and evolution of the North China craton, https://doi.org/10.1144/SP338.12, 2010.

Zhai, M.-G. and Santosh, M.: The early Precambrian odyssey of the North China Craton: A synoptic overview, Gondwana Research, 20, 6–25, https://doi.org/10.1016/j.gr.2011.02.005, 2011.

Zhang, C., Li, C., Deng, H., Liu, Y., Liu, L., Wei, B., Li, H., and Liu, Z.: Mesozoic contraction deformation in the Yanshan and northern Taihang mountains and its implications to the destruction of the North China Craton, Sci. China Earth Sci., 54, 798–822, https://doi.org/10.1007/s11430-011-4180-7, 2011.

Zhang, Y., Ma, Y., Yang, N., Shi, W., and Dong, S.: Cenozoic extensional stress evolution in North China, Journal of Geodynamics, 36, 591–613, https://doi.org/10.1016/j.jog.2003.08.001, 2003.

Zhang, Y., Dong, S., Zhao, Y., and Zhang, T.: Jurassic Tectonics of North China: A Synthetic View, Acta Geologica Sinica - English Edition, 82, 310–326, https://doi.org/10.1111/j.1755-6724.2008.tb00581.x, 2008.

Zhang, Y. Q., Mercier, J. L., and Vergély, P.: Extension in the graben systems around the Ordos (China), and its contribution to the extrusion tectonics of south China with respect to Gobi-Mongolia, Tectonophysics, 285, 41–75, https://doi.org/10.1016/S0040-1951(97)00170-4, 1998.

Zhao, G., Min, S., Wilde, S. A., and Sanzhong, L.: Late Archean to Paleoproterozoic evolution of the North China Craton: key issues revisited, Precambrian Research, 136, 177–202, https://doi.org/10.1016/j.precamres.2004.10.002, 2005.

Zhao, L. and Zheng, T.: Using shear wave splitting measurements to investigate the upper mantle anisotropy beneath the North China Craton: Distinct variation from east to west, Geophysical Research Letters, 32, https://doi.org/10.1029/2005GL022585, 2005.

Zhu, R., Xu, Y., Zhu, G., Zhang, H., Xia, Q., and Zheng, T.: Destruction of the North China Craton, Sci. China Earth Sci., 55, 1565–1587, https://doi.org/10.1007/s11430-012-4516-y, 2012.

Ziegler, P. A. and Cloetingh, S.: Dynamic processes controlling evolution of rifted basins, Earth-Science Reviews, 64, 1–50, https://doi.org/10.1016/S0012-8252(03)00041-2, 2004.

Zwaan, F. and Schreurs, G.: How oblique extension and structural inheritance influence rift segment interaction: Insights from 4D analog models, Interpretation, 5, SD119–SD138, https://doi.org/10.1190/INT-2016-0063.1, 2017.

Zwaan, F., Schreurs, G., Naliboff, J., and Buiter, S. J. H.: Insights into the effects of oblique extension on continental rift interaction from 3D analogue and numerical models, Tectonophysics, 693, 239–260, https://doi.org/10.1016/j.tecto.2016.02.036, 2016.

Zwaan, F., Chenin, P., Erratt, D., Manatschal, G., and Schreurs, G.: Competition between 3D structural inheritance and kinematics during rifting: Insights from analogue models, Basin Research, 34, 824–854, https://doi.org/10.1111/bre.12642, 2022.